A Spatial Frame Toy Model: Time, Gravity, and Cosmic Expansion from a Cavitating Four-Dimensional Void

Kepler Gelotte
Independent researcher
kepler.e.gelotte@gmail.com

July 27, 2026

Abstract

We present a geometric toy model in which three-dimensional space is a foam of Planck-scale cells continuously created by cavitation from a surrounding four-dimensional void. Successive completed generations of cells form *frames*. Only one current frame exists. Frame production sweeps all matter forward together, and each object carries a processed-frame register that accumulates fractionally: an object at rest in the substrate engages each passing frame fully, while a moving object *skims* its frames, registering each with the reduced weight $\sqrt{1 - w^2/c^2}$ set by its speed w relative to the cells, down to the null limit in which every frame passes wholly unregistered. The register's continuous ledger value $\mathcal{N}_{\text{proc}}$ against distance traversed advances at the fixed Euclidean rate c. Proper time is the ledger's frame-axis component, and time dilation is the cosine of the ledger's tilt, equivalently the accumulated skim deficit.

From two postulates formalizing this picture we prove a conditional chronometry theorem: for an ideal point clock following a piecewise-smooth timelike path through a region of uniform cell flow, evaluated in flow-rest coordinates, the smooth register equals standard Minkowski proper time. The square-root projection law is assumed rather than derived from cell mechanics. The theorem fixes elapsed time along clock worldlines; it does not by itself derive Lorentz transformations, relativity of simultaneity, or the dynamics of rulers, light, fields, and real composite clocks. The substrate rest frame is separately hypothesized to coincide with the CMB frame. It is absent from the ideal point-clock proper-time functional, but wider substrate invisibility requires additional matter and signal dynamics.

A third postulate, configuration tilt, extends the projection to extended bodies: a moving body's rest configuration lies along its ledger, so its footprint in the current frame is contracted by the same cosine that dilates its clock. It is selected by Michelson–Morley interferometry, and its cell-level mechanism is likewise open.

Descent between completed frames is defined by volume coverage rather than vertex parentage. A cell in frame $n + 1$ is a descendant of a cell in frame n when their interiors overlap with positive volume. The resulting weighted overlap graph is total: because every completed frame covers the same region without gaps, every parent volume is apportioned among one or more descendants, so geometrical descent cannot become extinct when vertex-nucleated candidates collapse (pop). The overlap rule supplies a candidate carrier for causal propagation and classical conserved quantities; a normalization-preserving quantum state-transfer rule remains open.

The action of a point mass is a pure effective frame measure, $S = -\hbar\,(m/m_P)\,\mathcal{N}_{\text{proc}}$, which rewrites standard quantum phase accumulation as a fixed Planck-unit phase increment per processed frame: each unit of the register rotates an object's internal phase by its mass in Planck units. Cells migrate laterally to fill voids left by popping, so the coarse-grained cell motion defines a flowing medium, and enhanced popping near mass was proposed to drive a steady inflow. The resulting chronometry is the Painlevé–Gullstrand ("river") metric, which for the inflow profile $v = \sqrt{2GM/r}$ is exactly the Schwarzschild geometry.

A pre-registered campaign in a hardened three-dimensional medium tested that flow mechanism and measured a negative result: a sustained sink refills by local nucleation and drives no inward flow. A second pre-registered campaign tested retarded nucleation as a static-substrate alternative and measured $\eta_0 = 0.605 \pm 0.058$, where full light deflection requires 3; its predicted solar-limb deflection of $1.05''$ contradicts the observed $1.75''$. Both negative results leave the chronometry theorem untouched and convert the gravity sector into a search under stated constraints.

Expansion proceeds in two modes. A timeless lateral growth of the foam addresses the horizon problem usually assigned to inflation, without a clock; where lateral pressure saturates, new cells extrude into the fourth dimension, beginning frame production and the onset of time. The visible universe is a spatially flat mode-2 region. That sector carries no expansion dynamics, and a third negative result is recorded in it: the proposed packing-statistics origin of primordial perturbations underpredicts their amplitude by forty-six orders of magnitude. Speculative extensions concerning pair creation, a mirror antimatter universe, a zero-point ledger, and a transactional quantum lock are kept separate from the core and stated with their open mechanisms and experimental boundaries.

Repository note

This version is a dated working paper released for timestamping, critique, and reproducibility. It is not peer reviewed. Following independent technical review, the chronometry claim is stated narrowly as an ideal-point-clock theorem, its coordinate and continuum conditions are explicit, and descent has been returned from vertex tethering to the original volume-covering definition. The discrete "skip" language of earlier versions is replaced throughout by fractional *skim* passage, matching the smooth register: frames register with a graded weight rather than a binary hit-or-miss. A follow-up consistency review prompted four further changes: an explicit status note on the gravity section (under active revision pending carrier simulations), restatement of the extremal-motion law as a postulate with a geodesic-equivalence theorem, a narrowed Planck-constant claim (an exact per-frame representation of quantum phase, with the conserved rotor action $J_0 = \hbar$ recorded as the open derivation standard), and fixed-total-energy phrasing for the source postulate's temperature clause. The core chronometry result remains a theorem conditional on the stated postulates. Two pre-registered campaigns have concluded with negative results: the round-8 certified-medium campaign (2026-07-16) for the flow-route gravity mechanism, and the retardation campaign (2026-07-20) for the retarded-nucleation microphysics of the static-substrate route. Sec. 5.3 reports both measurements, the claim-status table (Sec. 9) grades them, and Table 1 marks the fired rows. A third negative result is recorded in Sec. 6: the packing-statistics origin of primordial perturbations is falsified on amplitude, and the expansion-history claim of earlier versions is withdrawn. The speculative extensions in Sec. 7 set research targets for later work.

Contents

1 Introduction: the physical picture

This paper develops a single geometric idea. Space is a substance, not a passive container: a foam of Planck-scale cells, packed like bubbles, continuously created at its boundary by the negative pressure of a surrounding four-dimensional void. Each completed generation of cells is a *frame*. Time is not a background parameter in which this happens; time *is* identified with frame passage through matter. An ideal point clock is modeled by the smooth processed-frame register defined in Sec. 3.2; extending that rule to real composite clocks is a separate dynamical claim.

Three consequences, developed below, give the model its content.

First, **given a single advance postulate, ideal-clock chronometry becomes a theorem about projection** (Sec. 3). Every ideal point clock is assigned a smooth processed-frame register whose fixed Euclidean advance decomposes into temporal and spatial components. In flow-rest coordinates an object at rest advances purely along the register axis and ages fastest; motion tilts the ledger and reduces its temporal projection. The resulting elapsed time is exactly the Minkowski proper-time functional. This is a conditional consistency theorem, not a derivation of the square-root law from cell mechanics and not yet a derivation of the Lorentz transformations or of the dynamics of rods, light, fields, and composite clocks.

Second, **the gravity proposal is a flow** (Sec. 5). Cells pop under pressure, and energy (all energy, by a single coupling) enhances popping. Neighboring cells would migrate laterally to fill the voids, so around any mass the foam would drift steadily inward. Objects comoving with the drift are in free fall; objects held static must move against the current and suffer special-relativistic time dilation relative to it. If the medium supplies the inflow profile $v = \sqrt{2GM/r}$, the chronometry reproduces the Schwarzschild geometry *exactly*, with full light deflection, full Shapiro delay, and horizons where the current reaches one cell per tick. The entire content of static Newtonian gravity compresses into one falsifiable number, the exponent of the steady-state inflow around a popping-enhanced region; the moving-source sector adds a second, matched target, the null-limit wake asymmetry of Sec. 5.5. Both routes have now been measured. The certified-medium campaign found no steady inflow around a sustained sink; the flow mechanism stands falsified in that constitutive family. The retardation campaign then tested the static route's first candidate microphysics and measured a genuine two-dial response, a slower clock and denser space together, at a fixed ratio near 0.6 where full deflection demands 3 (Sec. 5.3). The weak-field burden now rests on a carrier no probe has yet found, and Sec. 5.3 records the constraints any successor must satisfy.

Third, **cosmic expansion has two modes, and time has a beginning** (Sec. 6). The foam first grows laterally in three dimensions, a mode with succession (generation follows generation) but no frames passing through matter and hence, by the model's own chronometry, no duration, which addresses the horizon problem usually assigned to inflation. Where lateral pressure saturates, new volume is forced into the fourth dimension: frame production begins, and with it, time. The visible universe lies deep inside such a frame-producing region, spatially flat as observed. This is an ontology, not a cosmology: Sec. 6 records that the sector supplies no expansion dynamics, and that the packing-statistics origin proposed there for primordial perturbations is falsified on amplitude.

Sec. 7 collects the speculative extensions: pair creation at popping, the mirror antimatter universe, the zero-point/dark-energy ledger, and a transactional lock mechanism for quantum events. Each is stated with its experimental boundary conditions and falsifiable targets, and each is separable: the chronometry, gravity, and expansion sectors stand or fall independently of anything in Sec. 7.

The presentation is geometric: each formal statement is paired with the picture that motivates it. The model maintains an honest ledger with experiment; Sec. 8 lists the measurements that have already pruned earlier versions of these ideas and that constrain all future extensions. For a reader who wants the model's exposure summarized before any of its machinery, Table 1 collects the kill conditions (Appendix A collects the notation): each row names a measurement — most of them runnable in simulation on the model's own substrate — whose stated outcome falsifies the indicated sector as formulated.

Sector	Falsified if
Emergent light cones (Sec. 2.3)	volume-overlap descendant cones fail to approach rotational isotropy, or the one-frame locality bound fails to yield a macroscopic limiting speed c under coarse-graining.
Gravity engine (Sec. 5)	material-marker chains in the historical flow-route implementation fail to lean around a popping-enhanced region (healing is in-place, not migratory). **Fired 2026-07-16**: the certified-medium campaign measured in-place healing around both a one-shot cavity and a sustained drain (Sec. 5.3).
Newtonian limit (Sec. 5.3)	the steady-state inflow exponent departs from $-1/2$ (e.g. relaxes to the point-sink r^{-2}), or the measured consumption density fails to match the divergence of the measured flow. Subsumed for the certified medium by the fired row above: no steady inflow exists to fit.
Static-substrate transducer (Sec. 5.3)	the linear-response ratio between cell-count excess and tick deficit departs from $\eta_0 = 3$ (equivalently $\varphi_\ell \neq \varphi_\nu$), so the predicted deflection $0.876'' \, (1 + \eta_0/3)$ contradicts the observed $1.75''$. **Fired 2026-07-20**: the retardation campaign measured $\eta_0 = 0.605 \pm 0.058$, predicting $1.05''$ (Sec. 5.3).
Constitutive closure (Sec. 5)	the pressure deficit around a sink is non-harmonic under the foam's own microdynamics. A post-hoc probe in the retardation campaign measured the pressure response around a drive as screened ($\lambda \approx 2.3$ spacings) plus a gradientless global offset, with no harmonic component; a pre-registered confirmation has not run.
Moving and null sources (Sec. 5.5)	the wake attracts co-moving light, or fails to double the pull on counter-propagating light (solar-limb deflection; Tolman–Ehrenfest–Podolsky).
Vacuum sector (Sec. 7.2)	the coarse-grained pop spectrum departs from ω^3, or the cutoff fails observer-independence: the substrate becomes visible.
Primordial perturbations (Sec. 6)	$S(k)$ of the saturated foam is not near-linear at small k, or the frozen packing statistics fail to deliver the observed fluctuation amplitude. **Fired 2026-07-29**: hyperuniform packing statistics give $\delta \sim 7 \times 10^{-52}$ at the comoving megaparsec scale against the required 10^{-5}, a shortfall of forty-six orders (Sec. 6).
Quantum sector (Sec. 7)	the single-particle Malus rule $\cos^2(\theta/2)$ cannot be derived from the quadratic lock rule (the Born and Bell targets collapse with it).
One-way sector (Sec. 3.8)	a synchronization-invariant disagreement among slow clock transport, light-exchange synchronization, two-way propagation, or boost composition, correlated with substrate velocity; any confirmed instance kills the exact postulate sector and standard relativity together, through the departure channels of Sec. 8.

Table 1: Kill conditions by sector. Chronometry (Sec. 3) enters only through the one-way row: by Theorem 1 it is exactly Minkowski, so it can only fail where special relativity itself fails, and Sec. 3.8 names the channel where both fail together.

2 The substrate: cells, frames, and the void

2.1 Cavitation from the Void

The primitive entities are *cells*: regions of space of characteristic linear size the Planck length, $\ell_P = \sqrt{\hbar G/c^3} = 1.616 \times 10^{-35}$ m. Cells are surrounded by, and embedded in, a four-dimensional *void* that exerts a persistent negative pressure on the foam, a tension that favors the creation of new volume, in the manner of cavitation in a fluid under tension.

New cells nucleate at the vertices formed between existing cells, the interstices, where the void's negative pressure is most concentrated. A nucleated cell that survives grows to a fixed maximum size, the Planck length, and then stops; growth is not open-ended. Within a generation, cells migrate until the closing frame is gapless, and the next generation then nucleates at the vertices of the completed frame. A cell crowded by its neighbors, however, can exceed the pressure threshold *before* reaching full size, and it *pops*: it is destroyed, returning its volume to the void. Popping is the dominant fate of nucleated candidates, not a rare accident: a completed frame has fewer cells than the previous frame had vertices, so most nucleations must pop for the frame to close gapless (Sec. 7.2 makes this quantitative: roughly six candidates are minted per surviving cell per frame). Figure 1 shows the *net* picture, the surviving tessellation with one pop in progress; the gross churn beneath it is taken up in Sec. 7. The core model does not need to answer whether a pop releases anything beyond its returned volume; a speculative extension in which each pop mints a matter–antimatter pair is developed in Sec. 7.1. Creation and destruction together maintain the foam near its natural density of one cell per Planck volume,

$$n_0 \simeq \frac{1}{\ell_P^3} \simeq 2.37 \times 10^{104} \text{ cells m}^{-3}. \tag{1}$$

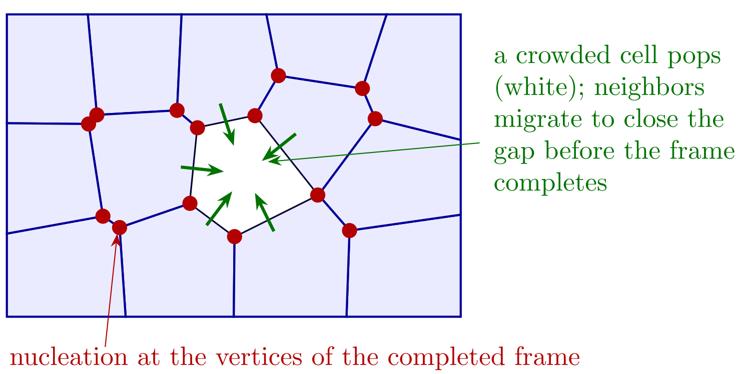

Figure 1: A frame of the cell foam in cross-section: a *gapless* tessellation. Cells grow to fixed maximum size and stop; a completed frame has no interstitial space, and the next generation nucleates at the vertices (red), where the void's negative pressure is most concentrated. A cell crowded past the pressure threshold before reaching full size collapses (white); its neighbors migrate laterally (green) to close the gap, so the frame closes gapless, the proposed origin of the cell flow in the historical gravity mechanism of Sec. 5. The only open boundary anywhere in the foam is the outermost mode-1 rim (Sec. 2.2).

2.2 Two modes of expansion and the onset of time

A *frame* is a completed Planck-thick generation of cells. Frames are produced at the universal rate

$$F_0 \;=\; \frac{1}{t_P} \;=\; \frac{c}{\ell_P} \;\simeq\; 1.8549 \times 10^{43} \text{ frames s}^{-1}, \qquad t_P = 5.391 \times 10^{-44} \text{ s}, \tag{2}$$

but frame production is not the foam's only way to grow. The chronometry construction itself requires only a fundamental length ℓ_0 and tick t_0 with $\ell_0/t_0 = c$; identifying these with ℓ_P and t_P is an additional physical hypothesis motivated by the later action, quantum, and gravity bridges, not a result of the special-relativistic calculation. The model has two modes of expansion, and the distinction between them is the distinction between timelessness and time.

Mode 1: lateral growth. Where the foam has room, cavitation simply enlarges it within its own three dimensions: new cells nucleate, the foam spreads, and no frames are produced. A distinction must be drawn carefully here, because the model will lean on it. Mode 1 possesses *succession*, since generation follows generation and statements like "a cell nucleates, grows, and pops" are ordered by that succession, but it possesses no *duration*: since time *is* frame passage (Postulate 2 below), and no frames pass through anything in mode 1, nothing in mode 1 has a clock, and the phase is not "brief" or "long." Whatever is said of mode 1 must be sayable in the language of generation order alone; in particular, all matter dynamics is frame passage (Postulate 2), so any matter present in mode 1 is *frozen inventory*: it can be separated by intervening nucleation, but it cannot act, interact, or decay. As Sec. 6 develops, this clockless lateral mode addresses the horizon problem usually assigned to cosmic inflation.

Mode 2: extrusion into the fourth dimension. Where the foam is hemmed in (cells under too much lateral pressure to spread, yet below the popping threshold), the void's tension still creates volume, and the only direction left is the fourth. New cells are forced out of the 3D layer, stacking a fresh Planck-thick generation atop the old: *frame production.* The first frame so produced is the onset of time. "Before" it, mode-1 growth already supplies succession: generation order without metric duration. Before frame production there was succession without proper time, so what is ill-posed about "what happened before" is not the ordering of events but the assignment of durations to them. The 4D structure of accumulated frames grows from that moment at one layer per tick.

Extrusion need not choose a side: a mirror stack can grow in $-F$ (Fig. 2); its interpretation is taken up in Sec. 7.1.

The visible universe lies deep inside a mode-2 region. Lateral mode-1 growth may continue at the rim of the saturated zone, but the rim lies beyond our horizon and plays no role in what we observe. In the frame direction, every point of 3D space borders the void: the present frame is the growing surface of the stack, everywhere, and *all matter resides in it*; the accumulated past frames carry no matter, and no object lingers in them (Sec. 3.1). (Whether anything *else* persists in past frames is a question the core model does not need to answer; the speculative lock mechanism of Sec. 7 proposes that instantiated energy does, and that amendment stands or falls with that section.) There is no observable "edge of space"; the only edges are the unobservable lateral rim and the frame-direction surface on which we live.

At laboratory and even galactic scales the relevant geometry is the stack: a *block* with Euclidean coordinates (F, x, y, z), where the frame-layer coordinate F counts completed frames along the frame axis (a distance $F\ell_P$). F is the *actual* stack coordinate: frame production advances every object's F by one layer per tick regardless of its motion. It is therefore distinct from the processed register σ of Sec. 3, which advances at a motion-dependent rate; the symbol

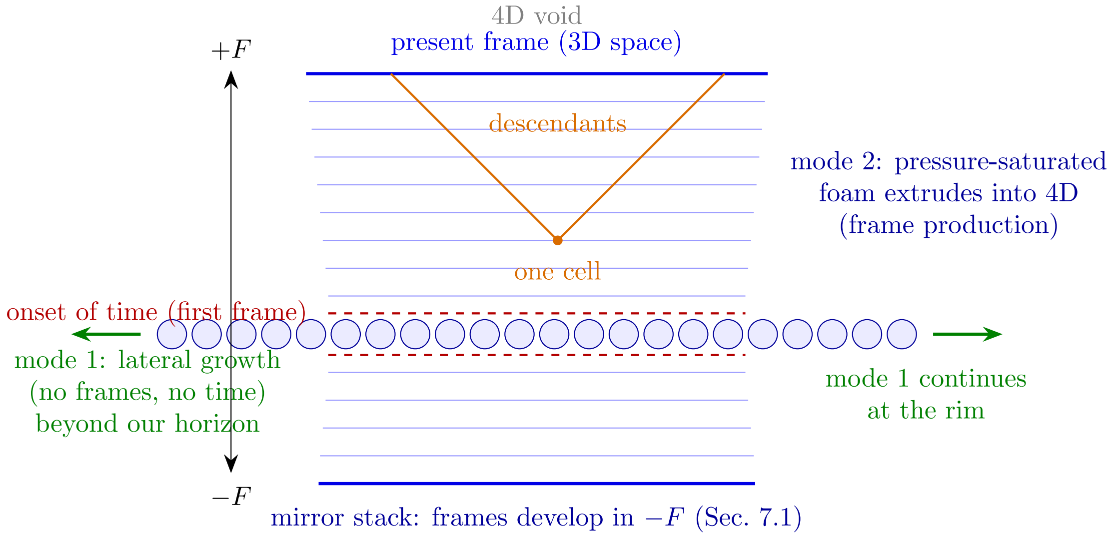

Figure 2: The two modes of expansion (one spatial dimension shown). The foam grows laterally without producing frames (mode 1, green): a timeless phase. Where lateral pressure saturates, new volume is forced into the fourth dimension (mode 2, blue): frames stack, and time begins at the first layer (red dashed). Extrusion can proceed in both four-dimensional directions, producing a mirror stack in $-F$; its speculative reading as an antimatter partner universe is developed in Sec. 7.1. The visible universe is deep inside the $+F$ stack; the lateral rim is beyond our horizon. The volume-overlap descendants of a single cell (orange) can extend by at most roughly one cell layer per tick. Their coarse-grained cone is the model's candidate light cone, with isotropy and exact limiting speed left as convergence tests in Sec. 2.3.

σ is reserved for that register throughout. We work in the block for kinematics (Sec. 3) and return to the two-mode picture for cosmology (Sec. 6).

2.3 Volume-covering descent and causal continuity

To speak of "the same place" in two successive completed frames, the model needs a rule of descent that survives popping and remeshing. Let $C_i^{(n)}$ denote cell i in frame n. The rule is geometric:

> *A cell $C_j^{(n+1)}$ is a descendant of $C_i^{(n)}$ when their interiors overlap with positive three-volume.*

Vertex nucleation remains the proposed mechanism by which candidates are created, but it no longer defines ancestry. A vertex-born candidate may pop before the next frame closes; descent is assigned only after the completed, gapless tessellation is known.

The relation is usefully recorded by the overlap weights

$$D_{ij}^{(n)} \equiv \frac{\mathrm{Vol}\left(C_i^{(n)} \cap C_j^{(n+1)}\right)}{\mathrm{Vol}\left(C_i^{(n)}\right)}. \tag{3}$$

For a completed next frame covering the same region without gaps,

$$D_{ij}^{(n)} \geq 0, \qquad \sum_j D_{ij}^{(n)} = 1. \tag{4}$$

Thus every parent of positive volume has at least one descendant. The structure is generally a many-to-many weighted graph: one parent volume may be divided among several children, and one child may overlap several parents. Unlike a vertex-tethered branching forest, this descent relation cannot become extinct merely because all immediate vertex-nucleated candidates pop.

The overlap graph supplies a precise coarse-grained continuity map. If $Q_i^{(n)}$ is an additive, cell-integrated classical quantity, the minimal conservative transport rule is

$$Q_j^{(n+1)} = \sum_i D_{ij}^{(n)} Q_i^{(n)}, \qquad \sum_j Q_j^{(n+1)} = \sum_i Q_i^{(n)}. \tag{5}$$

This is sufficient to state how classical density, charge, or a tracer measure is carried through remeshing. It is not yet a quantum state transfer law. A quantum implementation must preserve norms and correlations across the many-to-many map without copying an unknown state into every descendant; a unitary or isometric cell-level update is therefore an open microphysical requirement.

The overlap map fixes a rest frame without fixing a material velocity field. Its kernel is drift-free under near-isometric site motion: descendant barycenters track the parent volume rather than the moving cells, so barycentric transport reads zero velocity in the frame of the tiling itself, and that frame, the volume-rest frame, is the candidate substrate rest frame. A material cell-flow congruence, if a successor mechanism requires one, must come from site trajectories, material markers, or another dynamical variable; the overlap weights cannot supply it. Identifying that rest frame with the frame in which the cosmic microwave background is isotropic is a separate hypothesis of the larger model, not a consequence of the descent rule or of the chronometry theorem.

Descendant cones as candidate light cones. A child overlaps its parent but may extend beyond the parent's boundary by at most a cell scale. Because surviving cells have characteristic maximum size ℓ_P, one overlap step is local to approximately one cell layer. Iterating the relation therefore gives a microscopic causal bound of order one cell per frame, $\ell_P/t_P = c$. Equality and rotational isotropy at macroscopic scales are convergence claims, not consequences of positive overlap alone. The convergence rate has now been measured (Fig. 4). In the live remeshing rig (overlap descent sampled at cell sites and Voronoi vertices; roundness defined as $1 - \mathrm{CoV}$ of the boundary-mesh vertex radii about their centroid, a statistic that climbs toward 1 for a true sphere while a lattice cone stays pinned at its fixed faceting deficit), seeded runs at box sizes 18^3–56^3 cells (8, 6, 4, and 3 seeds) and a single 100^3 run together span cone populations $N \approx 8 \times 10^2$–2.5×10^5. Across that range the roundness deficit falls as a single power law,

$$1 - \mathcal{R}(N) \ \propto \ N^{-\alpha}, \qquad \alpha = 0.259 \pm 0.002 \quad \text{(47 points, 22 seeded simulations, five box sizes)}, \tag{6}$$

taking the deficit from 0.086 at $N \approx 2 \times 10^3$ to 0.024 at $N \approx 2.5 \times 10^5$, with per-run slopes between -0.248 and -0.277. In radius the law reads $1 - \mathcal{R} \propto R^{-0.78\pm0.01}$, consistent with a known mechanism: a ball grown by local stochastic surface addition is Eden growth, whose boundary roughens as a (2+1)-dimensional KPZ interface with growth exponent $\beta \approx 0.242$, so the relative roughness decays as $R^{\beta-1} \approx R^{-0.76}$ [20]. One exponent supports consistency with

KPZ/Eden roughening; a universality classification would take further scaling observables: height distributions, scaling collapse, a second exponent. On the present evidence the deficit behaves as transient interfacial roughening rather than fixed structural anisotropy.

Extrapolated under Eq. (6), the aggregate deficit is $\sim 3\times10^{-16}$ at nuclear scale and $\sim 6\times10^{-28}$ at one metre. That number sits far below the $\sim 10^{-17}$ scale of modern optical-cavity anisotropy bounds, but the two are not yet the same observable: $1-\mathcal{R}$ measures total radial boundary dispersion, the experiments constrain persistent directional structure in propagation speed, and the map from front geometry to effective signal velocity is undemonstrated. Three qualifications keep the claim honest. The extrapolation spans many decades beyond the measured window and rests on the universality identification rather than direct measurement. The rig is the May-generation medium (crowding pressure and Lloyd relaxation, without the later certified regulator), and its descent rule samples overlap at sites and vertices rather than computing exact overlap volumes; neither is expected to move the exponent, but neither has been re-measured on the certified rig. Most importantly, radius dispersion aggregates all multipoles: the Michelson–Morley-relevant residual is a *persistent* low-ℓ anisotropy that could in principle hide beneath the decaying roughness, and a spherical-harmonic decomposition of the front radius, tracking the $\ell = 2, 4$ amplitudes separately from the high-ℓ continuum, is the remaining instrument. (The lattice control shows the statistic detects such structure when it exists: at 0% disorder the cone grows a cube and the deficit does not decay.)

The limiting-speed half of that program now has its first measured piece. A displacement census with an exact overlap instrument, convex polyhedron clipping in which the descendants of each parent partition its volume with worst relative closure errors of 1.2–1.5×10^{-6} across the May-generation seeds and 7.7×10^{-7} on the certified medium, recorded every descent link over 150 consecutive frame pairs each: 1.9×10^{7} links per seed across three seeds on the May-generation rig and 5.2×10^{6} on the certified medium. Parent-to-descendant centroid displacements are short-ranged on both. Fitted to the exceedances above $\approx$1.9 spacings, the tail is thin, with exponential-class fits preferred at scales of 0.092–0.094 spacings across the May-generation seeds and 0.069 on the certified medium; the largest displacement among 6.2×10^{7} links is 2.98 spacings; and the observed per-run maxima sit at $+0.2$, -0.7, $+1.5$, and $+0.4$ standard deviations of the exponential extreme-value expectation, an unremarkable Gumbel sample. Read as a power law, the tail index lies between 21 and 31, the envelope of frame-pair bootstrap confidence intervals across the two media and fit depths, far above the $\mu \leq 2$ regime in which rare long links would make the iterated descent relation superdiffusive. In the tested runs, three seeds on the May-generation rig and one on the certified medium, a heavy-tailed single-step distribution is excluded as an obstruction: the observed tail does not rule out a finite limiting speed. The census does not measure that speed, its normalization, or its universality, and it does not constrain temporally or branch-correlated transport; those remain the open front-speed measurements. Data and instrument reside in the repository (`isotropy-campaign/`).

What remains to be demonstrated is therefore the absence of a persistent low-ℓ component; the convergence and normalization of the coarse-grained front speed, including correlated-transport effects, with the certified-medium census still single-seed. The roughness-convergence exponent and the single-step displacement tail are now measured quantities rather than assumptions.

The weighted overlap network, rather than a potentially extinguishing tethered tree, is used as the geometrical carrier of the speculative quantum propagation discussed in Sec. 7. The network guarantees continuity of support; the dynamical rule carried on that support remains a separate problem.

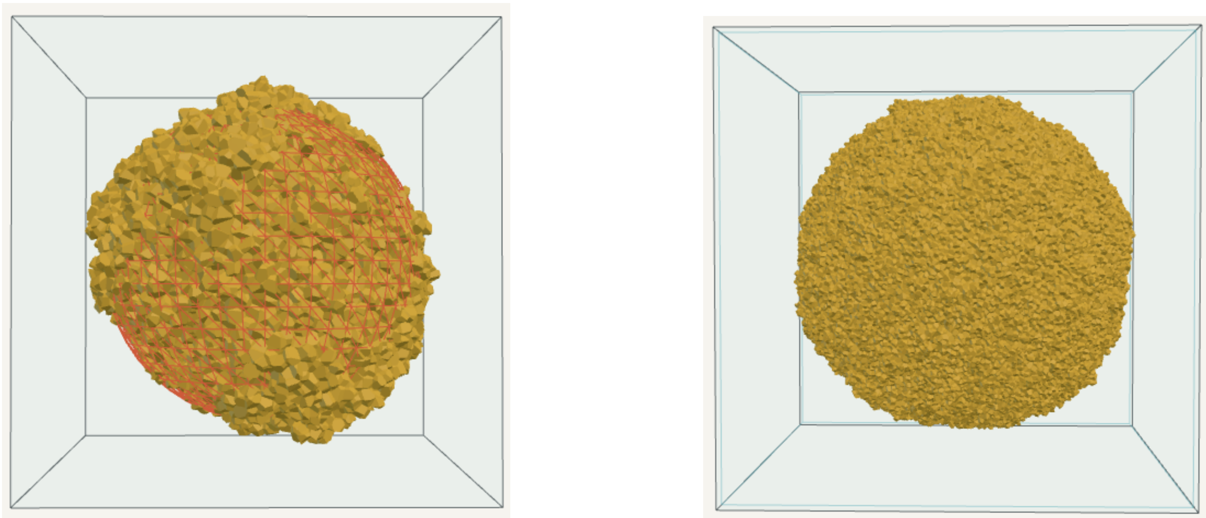

(a) $N \approx 1.7 \times 10^4$ cells

(b) $N \approx 2.7 \times 10^5$ cells

Figure 3: Causal-cone roundness convergence. *(a,b)* Overlap-descent cones on the live remeshing rig at two populations (illustrative single runs; red marks in (a) are descent links): macroscopically round, microscopically rough, with the relative roughness visibly shrinking.

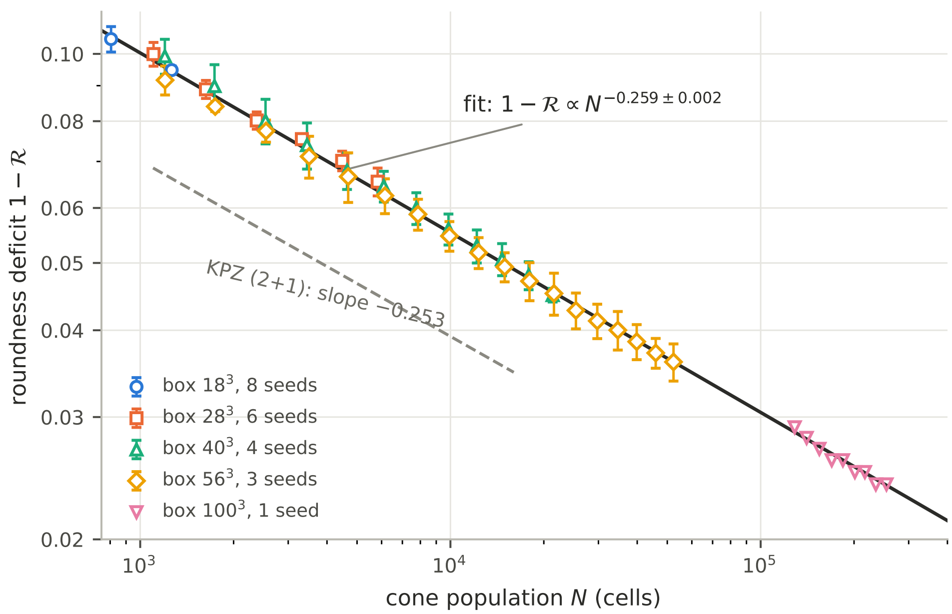

Figure 4: Roundness deficit $1 - \mathcal{R}$ against cone population for 22 seeded simulations in five box-size series; error bars are seed-to-seed standard deviations, and the single-seed 100^3 archival series carries none. The solid line is the weighted fit of Eq. (6), $1 - \mathcal{R} \propto N^{-0.259\pm0.002}$; the dashed reference shows the KPZ (2+1) slope -0.253. Data and fit script reside in the repository (`roundness-simulation/`).

3 Time as frame flux

3.1 The advance geometry: rotation, not subtraction

The central geometric claim requires two distinct statements.

The *actual* picture first: **there is only one current frame.** Frame production sweeps every object forward together, one cell layer per tick; nothing lags behind in the stack, and no object ever resides in a past frame. The present is universal: absolute simultaneity at the substrate level.

The *processed* picture is where clocks live. In this subsection v denotes speed relative to the local cells. Not every frame that sweeps through an object contributes a full unit to its processed register: a moving object *skims* the frames passing through it, each frame registering with a fractional weight rather than a binary hit-or-miss. Keeping the smooth effective register σ (in units of ℓ_P) against the spatial path length traversed gives the geometric law: **the processed ledger advances through the** (σ, x) **plane at the fixed Euclidean rate** c, so the processed component is, by Pythagoras,

$$\frac{\mathrm{d}\sigma}{\mathrm{d}t} \;=\; \sqrt{c^2 - v^2} \;=\; c\sqrt{1 - \frac{v^2}{c^2}}. \tag{7}$$

Time dilation is the cosine of a tilt angle in the ledger, equivalently the accumulated skim deficit. This is the model's geometric interpretation of the measured clock law; the cell-level mechanism producing the projection is not yet derived. An ideal clock at rest in the substrate engages every frame fully and accumulates the maximum register rate. The model separately hypothesizes that this substrate frame coincides with the CMB-isotropic frame. The formal null limit is the opposite extreme: at $v = c$ every frame is wholly skipped and $\mathrm{d}\tau = 0$. Interpreting that null limit as the behavior of physical light additionally requires the signal propagation dynamics left open in Remark 2.

3.2 Postulates

We now state the model's kinematic content precisely. Let t be substrate time, the global frame-production count multiplied by t_P. Let $\mathbf{v}(\mathbf{x})$ be the local cell-flow velocity in those substrate coordinates and

$$\mathbf{w} = \frac{\mathrm{d}\mathbf{x}}{\mathrm{d}t} - \mathbf{v}(\mathbf{x}) \tag{8}$$

be an object's velocity relative to the local cells.

The processed register used below is continuous. Denote its accumulated effective frame measure by $\mathcal{N}_{\mathrm{proc}} \in \mathbb{R}_{\geq 0}$ and set $\sigma = \ell_P \mathcal{N}_{\mathrm{proc}}$. In the language of Sec. 3.1, each frame contributes its fractional skim weight to this running accumulator. The microscopic mechanism that implements it remains open.

Postulate 1 (Ledger advance)**.** *Every elementary object's smooth processed register advances through the* $(\sigma, \mathbf{x})$ *ledger at the fixed Euclidean rate* c *with respect to substrate time:*

$$\left(\frac{\mathrm{d}\sigma}{\mathrm{d}t}\right)^2 + |\mathbf{w}|^2 = c^2. \tag{9}$$

The future-directed branch $\mathrm{d}\sigma/\mathrm{d}t \geq 0$ *is used.*

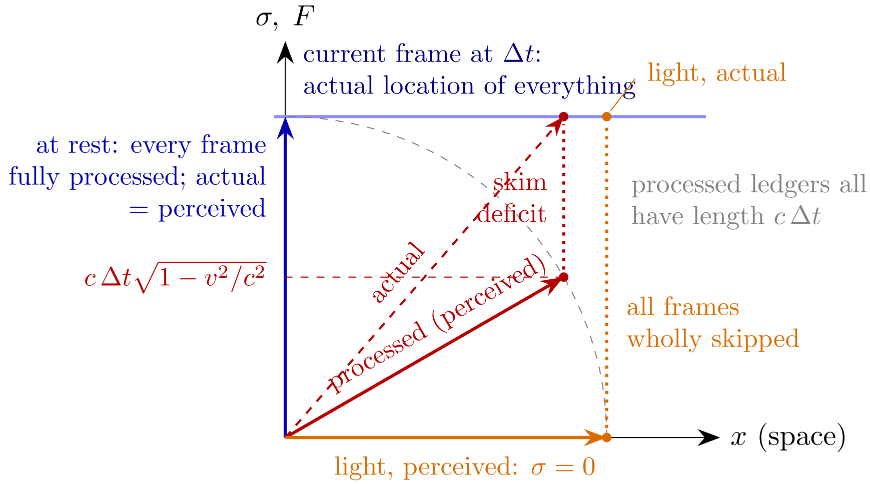

Figure 5: The advance geometry, separating the actual from the perceived. *Actual* (dashed, and the dots on the blue line): frame production sweeps everything to the single current frame, one layer per tick: there is only one present. *Processed* (solid): a moving object's effective processed register and spatial distance form a Euclidean ledger of length $c\,\Delta t$, so all ledgers end on the dashed circle; the dotted verticals mark the skim deficit. Rest maximizes processing; the orange horizontal leg is the formal null limit $d\tau = 0$, every frame wholly skipped. Time dilation is the accumulated skim deficit.

Postulate 2 (Chronometry)**.** *All physical dynamics is attributed by the model to frame passage. For an ideal point clock, elapsed proper time is the smooth processed-frame register:*

$$d\tau = t_P\, d\mathcal{N}_{\text{proc}} = \frac{d\sigma}{c}. \tag{10}$$

Clock increments are additive along piecewise-smooth segments of a worldline.

The first sentence of Postulate 2 is a broad ontological claim used elsewhere in the model. The chronometry theorem below uses only the ideal-clock identification and additivity. Motion never changes the processing rate per unit of the clock's own elapsed time, $d\mathcal{N}_{\text{proc}}/d\tau = 1/t_P$; it changes the amount of substrate time associated with a unit increase of the smooth register.

Remark 1 (The superseded subtraction rule)**.** *An earlier version of this model posited that the register rate followed a subtraction law, giving* $(1 - v/c)$*. That first-order dependence is excluded by optical-clock, Doppler, and storage-ring measurements. Binary processed/not-processed events do not themselves imply either the linear law or the square-root law: a binary sequence can realize any long-time fraction. For this reason the model treats frame passage as fractional (*skimming*) rather than binary (skipping): the register accumulates a graded weight per frame, so the discreteness of frames carries no statistical burden, and the open question is the value of the weight, not the selection of a sequence. The present projection rule is selected phenomenologically by experiment and installed in Postulate 1; deriving it from cell contact mechanics remains open.*

3.3 Ideal-clock Minkowski chronometry

Theorem 1 (Ideal-clock Minkowski chronometry)**.** *Consider an ideal point clock following a future-directed, piecewise-smooth timelike path through a region of uniform cell flow. Choose* *substrate coordinates comoving with that uniform flow, so that* $\mathbf{v} = 0$ *and* $\mathbf{w} = \mathrm{d}\mathbf{x}/\mathrm{d}t$*. Treat* $\mathcal{N}_{\mathrm{proc}}$ *as the smooth additive accumulator defined above. Then*

$$\tau[\mathbf{x}] = \int \sqrt{1 - \frac{|\dot{\mathbf{x}}|^2}{c^2}}\,\mathrm{d}t = \frac{1}{c}\int \sqrt{\eta_{\mu\nu}\,\mathrm{d}x^\mu \mathrm{d}x^\nu}, \tag{11}$$

where $x^\mu = (ct, \mathbf{x})$ *and* $\eta_{\mu\nu} = \mathrm{diag}(1, -1, -1, -1)$*. The formal null limit has* $\mathrm{d}\tau = 0$*.*

Proof. In the chosen flow-rest coordinates, Postulate 1 gives

$$\mathrm{d}\sigma^2 = c^2 \mathrm{d}t^2 - |\mathrm{d}\mathbf{x}|^2. \tag{12}$$

Postulate 2, the positive branch, and additivity then give

$$c^2 \mathrm{d}\tau^2 = c^2 \mathrm{d}t^2 - \mathrm{d}x^2 - \mathrm{d}y^2 - \mathrm{d}z^2, \tag{13}$$

and integration along the path yields Eq. (11). The proof does not begin with a Lorentzian spacetime metric, but it does assume a flat Euclidean spatial norm and the Euclidean ledger law of Postulate 1. The Minkowski quadratic form is the resulting rearrangement. □

Covariant rewriting. After Eq. (13) has been obtained, let u^μ denote the *dimensionless unit timelike vector* of the uniform cell flow, $\eta_{\mu\nu} u^\mu u^\nu = 1$; the corresponding dimensional four-velocity is $U^\mu = cu^\mu$. Decompose

$$\mathrm{d}x^\mu = (u_\nu \mathrm{d}x^\nu) u^\mu + \mathrm{d}x_\perp^\mu, \qquad c\,\mathrm{d}t \equiv u_\nu \mathrm{d}x^\nu, \qquad |\mathrm{d}\mathbf{x}|^2 \equiv -\eta_{\mu\nu}\mathrm{d}x_\perp^\mu \mathrm{d}x_\perp^\nu. \tag{14}$$

Recombining the split gives

$$(u\cdot\mathrm{d}x)^2 - \left[(u\cdot\mathrm{d}x)^2 - \eta_{\mu\nu}\mathrm{d}x^\mu \mathrm{d}x^\nu\right] = \eta_{\mu\nu}\mathrm{d}x^\mu \mathrm{d}x^\nu. \tag{15}$$

This is a covariant rewriting of the flow-rest result, not a second physical proof of general substrate invisibility: a vector's norm is unchanged when a chosen decomposition is recombined.

Corollary 1 (Ideal-clock reunion comparisons)**.** *For any two ideal point clocks sharing the same initial and final events, the age difference is the difference of their proper-time integrals in Eq. (11). In a uniform region, the straight timelike path between the events extremizes (and locally maximizes) the elapsed proper time.*

Remark 2 (Scope of the theorem)**.** *Postulate 1 already contains the measured square-root clock-rate law. Theorem 1 supplies a limited but real consistency result: it integrates that local rule along arbitrary piecewise-smooth timelike paths and recovers standard Minkowski proper time for ideal point clocks. It does not derive the projection law from cells, observer transformations, Einstein synchronization, relativity of simultaneity, or equations for light, fields, rods, interferometers, atoms, and other composite clocks. Length contraction is supplied separately by the configuration-tilt postulate of Sec. 3.6; it is installed there by experiment, not derived here. Those systems could, in principle, contain independent couplings to* u^μ *while retaining the point-clock functional above. Complete Lorentz–Poincaré equivalence therefore remains a target for the matter and signal sectors, not a consequence of this theorem alone.*

The smooth ideal-clock sector has no test distinct from special relativity: agreement with one is agreement with the other. Distinctive predictions would have to arise from a specified microscopic accumulator, discrete or correlated processing noise, non-clock dynamics, or another substrate coupling. Identifying the uniform cell-flow frame with the CMB frame is a separate hypothesis of the larger model.

Remark 3 (Simultaneity)**.** *The substrate ontology retains one current frame and hence an absolute slicing. Equation* (11) *alone supplies elapsed time along paths; it does not construct the Lorentz transformation or the moving observer's surfaces of equal operational time. A claim that Einstein relativity of simultaneity emerges at the processed level requires a separate synchronization and signal-propagation derivation; Sec. 3.7 carries this out at postulate level, conditional on isotropic signal propagation in the substrate frame.*

3.4 The twin paradox as block geometry

Figure 6 chooses the simplest flow-rest description: the home clock is comoving with the uniform substrate, while the traveler follows equal-speed outbound and inbound segments with an idealized turnaround. Both clocks occupy the one current frame at reunion, but their smooth registers differ. The home clock accumulates Δt; the traveler accumulates $\Delta t\sqrt{1-v^2/c^2}$ for the equal-speed segments and is younger by the standard special-relativistic amount. The age gap is the difference of the path integrals, not a difference between locations on the frame axis. Acceleration identifies where the traveler's path changes inertial segment, but it contributes no additional clock-slowing term beyond the proper-time integral and may be made arbitrarily brief. Scenario C of Sec. 3.5 sharpens the observation to its limit, deleting acceleration from the reunion altogether.

This example does not by itself establish the reciprocal descriptions or simultaneity assignments of arbitrary moving observers. Those require the observer transformations and signal conventions explicitly left open in Remark 2 and carried out at postulate level in Sec. 3.7. It also rests the home clock in the substrate, which a skeptical reader may suspect is load-bearing; Sec. 3.5 removes that convenience and runs the comparison with the home clock in motion.

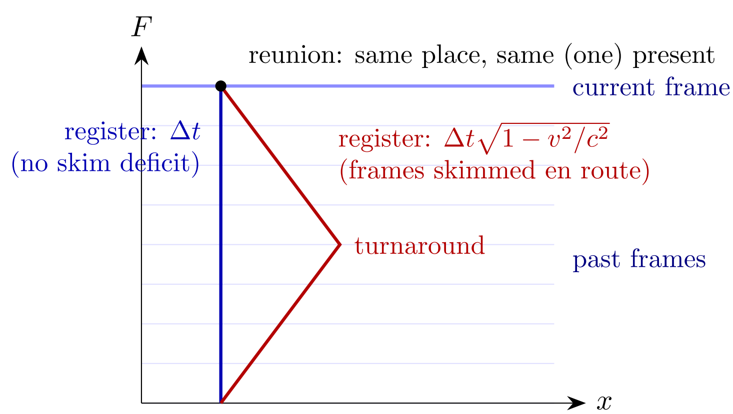

Figure 6: The twin paradox with one universal present. Both worldlines are swept upward one frame per tick and terminate together on the current frame; the traveler does not reside in an earlier frame. The age gap lives in the carried smooth registers: in these flow-rest coordinates the homebody engages every frame fully, while the traveler's tilted path skims frames en route and accumulates less proper time.

3.5 Twin reunions from a moving home frame

The example above rests the home clock in the substrate. That choice is a courtesy to the drawing, not a load-bearing assumption, and it is worth demonstrating as much: a skeptical reader will suspect that the model's account of the twins works only when the favored twin owns the preferred frame. By Theorem 1 and Corollary 1, reunion ages are Minkowski path integrals, and whichever twin's worldline between the shared separation and reunion events is straight ages the most, regardless of how either twin moves relative to the substrate. Three scenarios make this concrete. The first two are arranged so that the substrate-rest state belongs to the *traveler*: the configuration in which a preferred-frame model looks most likely to get the answer wrong. The third deletes acceleration from the comparison altogether.

Scenario A: visiting the preferred frame does not win the reunion. Let Earth cruise through the substrate at $u = 0.6c$, and let the traveler brake (idealized as brief) to *substrate rest*, coast for one substrate tick, then chase Earth down at $0.9c$ (Fig. 7, left). In units with $c = 1$ and ages in ticks, the substrate ledger reads:

	substrate time	traveler adds	Earth adds
leg 1: traveler at substrate rest	1.000	1.000	0.800
leg 2: traveler chases at $0.9c$	2.000	0.872	1.600
reunion totals	3.000	**1.872**	**2.400**

During leg 1 the traveler, at absolute rest, *genuinely ages faster*: every frame is fully processed while Earth skims at rate 0.800. The surplus of 0.200 ticks is real. But it is banked against a debt: rejoining a receding Earth means chasing at a speed necessarily greater than u, here $0.9c$, skimming hard for two substrate ticks and surrendering 0.728. The surplus is spent with interest, and the net deficit of 0.528 ticks is exactly the Minkowski value that any inertial frame computes for this pair of worldlines. Visiting the preferred frame bought the traveler faster aging while it lasted, and a younger face at the reunion.

Scenario B: the symmetry. Run the same first leg, but now at tick 1 the *Earth twin* changes their mind and flies back at $0.9c$ to the waiting traveler (Fig. 7, right). The traveler coasts at substrate rest throughout and ages 1.667 ticks; the Earth twin ages 0.800 on the outbound cruise and 0.291 on the return, totalling 1.091. The first legs of the two scenarios are identical tick for tick, yet the outcomes reverse: now the Earth twin is younger, by 0.576 ticks. What decides a reunion is not who ends at rest in the substrate but whose path between the shared events is bent, exactly as Corollary 1 requires.

Scenario C: Scenario A without acceleration. Scenario A's traveler performed two maneuvers, a brake and a chase, and neither is doing any work: the same reunion can be assembled from three clocks that never accelerate (Fig. 8). The comparison relays a register across two inertial clocks; no single clock ages through the whole path. Earth cruises at $u = 0.6c$ exactly as before. A clock B rests permanently in the substrate, coincident with Earth at the separation event, where it zeroes its register. A clock C cruises permanently at $0.9c$, timed to cross B's worldline at tick 1, where it copies B's register reading in passing, and to overtake Earth at tick 3. The ledger is column for column the ledger of Scenario A: B's leg banks 1.000, C's leg adds 0.872, and C draws level with Earth carrying 1.872 against Earth's 2.400. Nothing anywhere accelerated. By the additivity clause of Postulate 2, the handed-off register accumulates the same piecewise path integral as Scenario A's traveler, and that integral never contained an acceleration term to begin with. What acceleration supplied in Scenario A was transport, not physics: the means by which a single clock comes to occupy both legs of a bent path. The age gap belongs to the bent path itself, the skim deficit accumulated leg by leg through the cell flow, whether or not any single object traverses the whole of it.

Remark 4 (What is absolute and what is operational)**.** *The leg-by-leg columns above are absolute: the substrate assigns each clock a definite rate at every tick, and during the first leg of all three* *scenarios the cruising Earth genuinely ages slower than the substrate-resting clock. An Earth observer using Einstein-synchronized clocks would judge the receding traveler* slower *during that same leg. The two verdicts do not collide: they compare different pairs of distant events, differing by simultaneity convention, and Theorem 1 guarantees they agree on every reunion total, the only comparison that is convention-free. No clock-based experiment resolves the leg-by-leg attribution; constructing the moving observer's operational judgments in full (synchronization, reciprocity of descriptions) is carried out at postulate level in Sec. 3.7, within the scope limits of Remark 2. What the reunions establish is narrower but exact: The model's preferred frame confers no automatic reunion-age advantage. A twin who attains the substrate's own rest frame still loses the reunion comparison whenever their worldline is the bent one.*

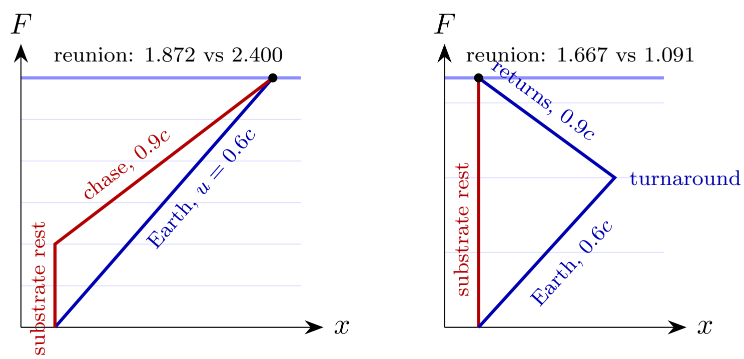

Figure 7: Twin reunions with the home clock in motion through the substrate ($u = 0.6c$; substrate coordinates; the two panels are not to a common scale). *Left, Scenario A:* the traveler (red) brakes to substrate rest, out-ages the cruising Earth (blue) for one tick, then chases at $0.9c$ and returns younger: 1.872 against Earth's 2.400. *Right, Scenario B:* identical first leg, but the Earth twin turns back at $0.9c$ instead; now Earth is younger, 1.091 against the resting traveler's 1.667. In both panels the straight worldline between the shared events wins the reunion (Corollary 1); residence in the preferred frame does not decide the reunion-age ordering.

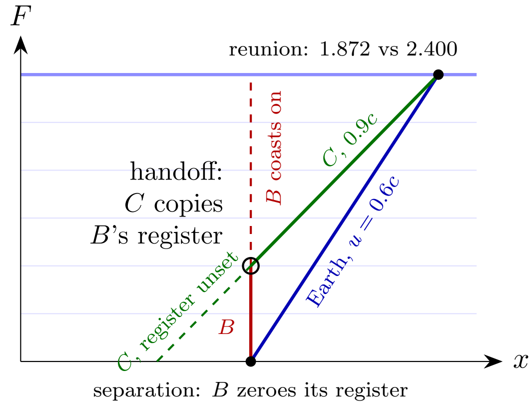

Figure 8: Scenario C: the register handoff (substrate coordinates; Earth cruises at $u = 0.6c$ exactly as in Scenario A). Three inertial worldlines replace Scenario A's bent traveler: clock B (red) rests in the substrate and zeroes its register at the separation event; clock C (green), cruising permanently at $0.9c$, copies B's register (its clock reading) as their worldlines cross (circle) and overtakes Earth (blue) carrying the total 1.872 against Earth's 2.400, exactly Scenario A's reunion ledger. The dashed segments contribute nothing to the comparison. No worldline bends: the age gap belongs to the bent path assembled from the two solid legs, not to any dynamical effect of acceleration on clocks.

Remark 5. *The effective processed-frame measure is* path-dependent*: it is the additive integral of the projection along the worldline, $\tau = \int \sqrt{1 - w^2/c^2}\,\mathrm{d}t$, not a function of net displacement. Two journeys covering the same total distance in the same total substrate time generally yield different proper times if their velocity profiles differ. (An earlier draft of this model asserted the contrary; the storage-ring muon, which circulates with zero net displacement while aging thirty times slower, settles the matter empirically.)*

3.6 Length contraction as configuration tilt

Postulates 1–2 constrain the register an object carries; they say nothing about the register's *neighbors*. An extended body is a set of constituents, and in the substrate ontology its length is a definite, absolute quantity: the span of cells the body occupies in the one current frame. Nothing in the ledger bookkeeping repositions constituents when the body moves. If a moving rod kept its cell span, the substrate would be detectable: a Michelson interferometer compares the two-way drive time along and across the motion, and with time dilation but no contraction the comparison is anisotropic at order w^2/c^2, excluded by Michelson–Morley-class experiments at the $\sim 10^{-17}$ level. Within this model, interferometry therefore *measures* a property of extended matter, exactly as optical clocks measure the square-root law of Postulate 1. We install what it measures as a third postulate.

Postulate 3 (Configuration tilt)**.** *The equilibrium configuration of an extended body moving at velocity $\mathbf{w}$ relative to the local cells lies along the body's ledger direction: the rest configuration is tilted by the ledger angle θ, with $\cos\theta = \sqrt{1 - |\mathbf{w}|^2/c^2}$, in the plane spanned by the frame axis and the motion. Its footprint in the current frame is therefore contracted along the motion,*

$$L \;=\; L_0\sqrt{1 - \frac{|\mathbf{w}|^2}{c^2}}, \tag{16}$$

where L_0 is the extent of the rest configuration, and is unchanged transverse to the motion.

One tilt, two projections: the same $\cos\theta$ that projects a constituent's advance onto the frame axis (time dilation, Eq. (7)) projects the body's configuration onto the current frame (length contraction, Eq. (16)). In the skim language of Sec. 3.1, all of a rigid body's constituents skim frames at the common rate fixed by $\mathbf{w}$, and Postulate 3 states that the body's shape rides the common tilt rather than standing upright in the ledger plane (Fig. 9). The transverse statement costs nothing: the tilt lives entirely in the $(\sigma, x_{\|})$ plane, so extent perpendicular to the motion has no leg to project.

Remark 6 (Status of the tilt postulate)**.** *Postulate 3 is a statement about matter, not about chronometry, and it is installed on the same epistemic footing as Postulate 1: selected by experiment, with the cell-level mechanism open. Michelson–Morley selects the contraction factor given the register law; Kennedy–Thorndike and Ives–Stilwell close the triangle, fixing the dilation–contraction pair to the relativistic values against alternatives that trade one against the other. What remains open is the constructive derivation: in the model's own terms, a body is a choreography pattern bound by drives propagating at c relative to the cells (Secs. 2.3, 7), and the Lorentz–FitzGerald route would obtain Eq.* (16) *as the equilibrium of such a pattern in motion. That derivation inherits the wave-sector convergence claims (isotropy and exact limiting speed of the overlap cones) and sits beside them on the open ledger. Until it is carried out, contraction here has the status of a measured projection rule, not a consequence of cell mechanics.*

Remark 7 (Geometric reciprocity)**.** *The projection is symmetric between ledgers (Fig. 9). Project a substrate-rest rod onto a moving observer's spatial axis — the direction orthogonal to that observer's ledger — and the same factor* $\cos\theta$ *appears: each party measures the* other's *rod contracted, with no asymmetry to exploit. But the identification of "the moving observer's spatial axis" with the orthogonal direction is doing operational work: it encodes which distant events the moving observer treats as simultaneous, i.e. a synchronization convention. Deriving that convention operationally (from slow clock transport, which Theorem 1 already governs, or from light exchange, which requires the signal sector) is the subject of the reciprocity construction covered in Sec. 3.7.*

3.7 Reciprocity: pairing, substrate accounting, and measurement

Remark 7 left a promise: geometric reciprocity becomes measured reciprocity only when the moving observer's synchronization convention is derived rather than assumed. This subsection discharges that promise at postulate level, and shows along the way why the ledger plane itself cannot be promoted to a frame transformation. Throughout, two ideal clocks a and b move collinearly through a region of uniform flow at $w_a = 0.6c$ and $w_b = 0.8c$, so that $\cos\theta_a = 0.8$ and $\cos\theta_b = 0.6$.

Three inequivalent accountings answer "how fast does the other clock run," and the model must keep them separate.

(i) Geometric pairing. After substrate time t both ledgers have Euclidean length ct; projecting either onto the other's direction gives $ct\cos(\theta_b - \theta_a)$, the same both ways. The symmetry is exact and exactly empty: it is the symmetry of the bilinear form, $\hat{u}_a \cdot \hat{u}_b = \hat{u}_b \cdot \hat{u}_a$, and would hold under any dynamics whatsoever, including physics with no time dilation at all. It also returns

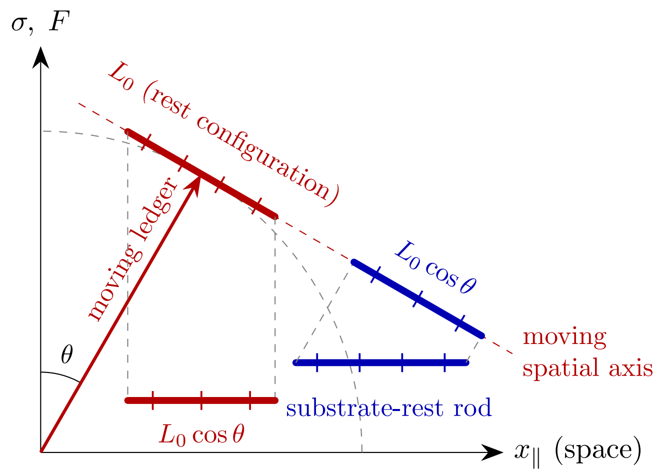

Figure 9: One tilt, two projections, both ways ($\cos\theta = \sqrt{1 - w^2/c^2}$). *Red, Case A:* a moving rod's rest configuration L_0 lies along its own spatial axis, the direction orthogonal to its ledger (Postulate 3); its footprint in the current frame is the vertical projection $L_0 \cos\theta$: the substrate observes the moving rod contracted. *Blue, Case B:* projecting a substrate-rest rod perpendicularly onto the moving spatial axis gives the same factor: the moving observer measures the substrate's rod contracted by exactly as much. The reciprocity is geometric here; reading the moving axis as the moving observer's simultaneity slice is a synchronization convention whose operational derivation is covered in Sec. 3.7. The projected magnitude survives that caveat because contraction is even in w: the operational measurement of Proposition 1 confirms $L_0 \cos\theta$ while replacing the slice itself.

the wrong number: $\cos(\theta_b - \theta_a) = 0.8 \times 0.6 + 0.6 \times 0.8 = 0.960$, where the measured mutual rate (accounting (iii)) is 0.923. And the two ledger tips being compared are *substrate-simultaneous* events, so the "perspective" in this construction is the substrate's, not a's or b's.

(ii) Substrate accounting. The registers advance at $\mathrm{d}\sigma/\mathrm{d}t = c\cos\theta$, so at equal substrate time the rates stand in the ratio $\cos\theta_b / \cos\theta_a = 0.750$: b genuinely accumulates less register than a, and the inverse comparison is 1.333. This accounting is asymmetric, and correctly so — the model has a preferred frame, and its internal bookkeeping does not pretend otherwise. But neither clock can perform it without access to substrate simultaneity.

(iii) Measurement. What each clock *can* do is synchronize distant clocks by two-way signal exchange and compare a passing clock against the synchronized pair. Proposition 1 shows that this procedure, executed with the model's own contracted rods and dilated clocks, returns the mutual rate $\sqrt{1 - w_{\mathrm{rel}}^2/c^2} = 0.923$ both ways, with $w_{\mathrm{rel}}/c = (0.8 - 0.6)/(1 - 0.48) = 0.385$ fixed by Einstein composition.

Accounting	a judges b	b judges a	reciprocal?
(i) mutual ledger projection	0.960	0.960	yes — vacuously
(ii) substrate rates $\cos\theta_b / \cos\theta_a$	0.750	1.333	no — correctly not
(iii) light-synchronized measurement	0.923	0.923	yes — and measured

Row (iii) is the only row an experiment sees; row (ii) is the only row the substrate sees; row (i) is a property of cosines.

Proposition 1 (Operational reciprocity)**.** *Assume, in addition to Postulates 1–3, that signals propagate isotropically at the fixed rate c in the substrate frame. Then clocks synchronized by two-way signal exchange on a platform moving at w measure the two-way signal speed to be exactly c; a clock moving at velocity* w_{rel} relative to the platform *(Einstein composition) to run at* $\sqrt{1-w_{\mathrm{rel}}^2/c^2}$*; and, in particular, two such platforms each judge the other's clocks slow by the same factor.*

Proof. Put two clocks at the ends of a rod of rest configuration L_0 aligned with the motion; its footprint in the current frame is $L_0 \cos\theta$ (Postulate 3). A forward signal takes substrate time $L_0 \cos\theta/(c-w) = \gamma(1+w/c)L_0/c$ and the return $L_0 \cos\theta/(c+w) = \gamma(1-w/c)L_0/c$, where $\gamma = 1/\cos\theta$: the round trip costs $2\gamma L_0/c$ of substrate time and hence, at register rate $\cos\theta$, exactly $2L_0/c$ of platform proper time — the two-way speed is c independent of w, which is why the platform cannot detect its own motion this way. The synchronization convention assigns each leg L_0/c, while the platform clocks actually accumulate $(1+w/c)L_0/c$ during the forward leg; the front clock is therefore set *behind* the rear clock by wL_0/c^2: leading clocks lag. Register rate $\cos\theta$, footprint $\cos\theta$, and offset $-wx'/c^2$ now assemble into exactly the Lorentz map between substrate and platform coordinates; composing two such maps composes velocities in the Einstein way, and between two platforms the mutual judged rate is $\sqrt{1-w_{\mathrm{rel}}^2/c^2}$, symmetrically. □

Reciprocity is therefore not a geometric fact in this model but a theorem about instruments [1]: it holds, with the measured value, because the conspiracy among rate, footprint, and synchronization offset is exact. The substrate asymmetry of accounting (ii) is real and invisible to every rod-and-clock protocol — which is precisely the bounded invisibility target of Remark 2, here reached for the signal sector at postulate level: the proposition is conditional on isotropic signal propagation in the substrate frame, an assumption of the signal sector, not a derived property of cells.

Remark 8 (Why projection cannot be promoted to a transformation)**.** *Three independent obstructions close the shortcut of reading the ledger plane as a frame transformation.* First*, σ is a path functional, not a coordinate: two worldlines through the same event carry different registers, so there is no shared (σ, x) chart in which one observer's axes could be rotated into another's; each worldline owns its plane.* Second*, the sign is wrong: the Euclidean-orthogonal slice through a moving ledger tip maps to the line $ct = -(\gamma w/c)\,x$ in substrate coordinates — slope* -0.750 *at* $0.6c$ *— where the synchronization offset derived in Proposition 1 tilts the other way, $ct = +(w/c)x$, slope* $+0.600$*. Orthogonal-slice simultaneity predicts leading clocks* lead*, and the sign of the offset is measurable.* Third*, the group is wrong: the circle's transformations are the compact* $SO(2)$*, whose angles add and wrap, while measured velocity composition is the non-compact* $SO(1,1)$*, whose rapidities add without bound. Composing* $0.8c$ *with* $0.8c$ *by angle addition gives* $\sin(2\theta) = 0.960$ *with* $\cos(2\theta) = -0.280$ *— a negative register rate — where Einstein composition gives* $0.976c$ *and a rate that never vanishes. The ledger plane is per-worldline bookkeeping for Postulate 1; the transformation group of measurements lives in the operational sector of Proposition 1. The proper-time-as-fourth-dimension literature [2] reached the same wall at the same place, and the model adopts its lesson rather than re-deriving it: draw each observer's plane separately, and transform only through instruments.*

3.8 One-way speeds and the edge of detectability

Proposition 1 pins the two-way speed of light at c on every platform. One-way speeds obey a weaker rule. A one-way value exists only after a synchronization convention pairs the distant clocks that timestamp departure and arrival; change the convention and the value changes, while the two-way average stays fixed [3]. Experiments constrain two-way speeds and the consistency of conventions. None reads a one-way speed off nature. The model spends this conventional freedom in one place: signals travel at c in every direction of the substrate frame, the standing assumption of Sec. 3.7, and each moving platform inherits its one-way values from that choice.

Substrate accounting makes the inheritance concrete. A platform moving at w chases the light it emits forward and meets the light it emits backward: the closing rates are $c-w$ and $c+w$, approaching 0 and $2c$ as $w \to c$. These are row (ii) statements in the sense of the table of Sec. 3.7: true in the substrate ledger, asymmetric, and out of reach of platform instruments. The row (iii) statement stands beside them without conflict: clocks synchronized by two-way exchange report one-way speed c in both directions, because the leading-clocks-lag offset wL_0/c^2 absorbs the closing-rate asymmetry. Slow clock transport yields the same pairing, since Theorem 1 governs the transported clock and its offset agrees with the light-exchange convention as the transport speed vanishes. The two conventions agree at every w, so comparing them exposes nothing.

The limit $w = c$ closes the sector. The footprint $L_0 \cos\theta$ vanishes, the register rate vanishes with it (the null limit $\mathrm{d}\tau = 0$ of Theorem 1), and the forward synchronization signal never arrives, since $L_0 \cos\theta/(c - w)$ diverges. No platform, no clocks, no convention. Talk of light "in its own frame" has no referent in this model; the extreme case belongs to substrate accounting alone, as the closing rates 0 and $2c$ between a null worldline and the observers it overtakes or meets.

The invisibility is conditional. Proposition 1 cancels the closing-rate asymmetry through three factors the postulates supply as exact: register rate $\cos\theta$, footprint $\cos\theta$, offset $-wx'/c^2$. Each departure channel of Sec. 8 perturbs at least one factor. A discrete or noisy accumulator perturbs the rate; an independent matter coupling to u^μ (Remark 2) perturbs the footprint; Planck-scale dispersion perturbs the signal legs. A perturbed factor becomes observable only as a synchronization-invariant inconsistency: a mismatch between light-exchange and slow-transport synchronization, an anisotropic two-way or closed-loop signal time, or a failure of the boost composition law. A bare one-way speed stays convention-dependent even then; the invariant is the disagreement among complete procedures. Any such residual would key to the laboratory's velocity through the substrate: under the frame hypothesis of Sec. 2.3, to the CMB dipole at 369 $\mathrm{km\,s^{-1}}$. The Robertson–Mansouri–Sexl test theory parametrizes the associated deviations in clock, rod, and two-way propagation behavior [4], and current bounds on its parameters constrain each candidate channel.

This sharpens the sector's standing in Table 1 without changing it. With the postulates exact, the chronometry fails only where special relativity fails, the ground on which the table exempts it. The one-way residual names the concrete channel where both would fail together and where the substrate frame would first show. The model's most distinctive commitment, one-frame isotropy of the one-way speed, carries no observational cost while the cancellation is exact, and produces a definite signature if any departure channel of Sec. 8 is real.

4 Geodesics and the quantum bridge

4.1 Free motion as stationary flux

Postulate 4 (Stationary register)**.** *Free configurations follow stationary processed-frame action: between fixed block events, a free body's worldline satisfies* $\delta\int \mathrm{d}\mathcal{N}_{\text{proc}} = 0$*.*

Theorem 2 (Geodesic equivalence)**.** *Given Postulate 4, Theorem 1 identifies the stationary-register principle with the geodesic principle* $\delta\int \mathrm{d}\tau = 0$*. In a homogeneous substrate the solutions are straight worldlines at constant velocity.*

The split matters for bookkeeping. Postulates 1–2 fix elapsed time *along* a path; they do not select which path a free body takes. The extremal law is an independent dynamical input, stated here as a postulate so that the equivalence above is not mistaken for a derivation of inertia from chronometry alone.

The action of a point mass is therefore a pure effective frame measure:

$$S \;=\; -mc^2\int \mathrm{d}\tau \;=\; -\hbar\,\frac{m}{m_P}\,\mathcal{N}_{\text{proc}}, \qquad m_P = \sqrt{\hbar c/G}, \tag{17}$$

using $\hbar = E_P t_P$. Inertia, in this reading, is the stationary-register postulate at work: a free object follows the path of stationary frame flux (Postulate 4, an independent dynamical input), and resisting that path forces a sub-optimal projection history.

4.2 Phase per frame: a Planck-unit representation of quantum phase

Equation (17) gives the path-integral weight the exact form

$$e^{iS/\hbar} \;=\; e^{-i\chi\mathcal{N}_{\text{proc}}}, \qquad \boxed{\chi = \frac{m}{m_P} \text{ radians per unit processed-frame measure.}} \tag{18}$$

Each unit increase of the smooth processed register rotates the object's internal phase by its mass in Planck units. Because m_P and t_P are themselves defined through $\hbar$, Eq. (18) is an exact Planck-unit rewriting of the standard Compton phase: a representation of quantum phase in per-frame form, not an independent explanation of why the action quantum has the value it does. One clarification, on which Sec. 5 will lean: Eq. (18) is the phase *along the worldline*: the action phase, the rate at which the object's own register turns, per unit processed-frame measure. The same phase field, evaluated at a fixed cell of the substrate as the object's pattern streams past, advances at the strictly greater rate $E/\hbar$ per unit substrate time; the two rates coincide only at rest, and their difference is taken up in Sec. 5, where it matters. Planck's constant never appears independently in the dynamics; only the dimensionless angle χ does. For the electron, $\chi = 4.185\times10^{-23}$ rad per frame, which at rest accumulates at $\chi/t_P = 7.763\times10^{20}$ rad s^{-1} $= m_e c^2/\hbar$, precisely the de Broglie–Compton internal frequency, completing one full cycle every $2\pi m_P/m_e = 1.501\times10^{23}$ frames. Along a classical trajectory the accumulated angle reproduces the on-shell de Broglie phase, since $Et - \mathbf{p}\cdot\mathbf{x} = mc^2\tau$ on shell; summing the per-frame rotations over *all* block paths supplies the phase each path carries in a Feynman path integral; the measure, normalization, and propagator remain underived, and stationary phase of the supplied weights recovers Theorem 2. Of the three textbook roles of $\hbar$, two, the action phase and the energy–frequency conversion, are exhibited by (18) plus the substrate kinematics; the third, the commutation scale, is conjectured to reduce to the same rotation but has not been derived, and the claim should be read with that boundary. What would upgrade the representation to an explanation is a conserved rotor action derived from cell mechanics: a mechanical state variable of the foam whose action is conserved under descendant propagation, quantized with a smallest nonzero excitation J_0, and universal across species, location, and history, with experiment then identifying $J_0 = \hbar$. That derivation is open and sits on the ledger beside the square-root law and the tilt mechanism. In this representation, rest mass sets the rotation rate: heavier objects twist faster per frame, which is why their interference fringes are finer and their classical limit closer.

5 Gravity as cell flow

Status of this section. This section documents the historical cell-flow gravity proposal: its exact Painlevé–Gullstrand correspondence and the constitutive mechanisms tested to date. The pre-registered campaigns returned negative results for both the flow route and retarded nucleation (Sec. 5.3), and the gravity ontology is under active revision, with volume-overlap descent (Sec. 2.3) and a conservation-protected mechanical carrier as successor candidates and dedicated simulations in progress. The mechanism prose below therefore retains the historical flow-route language (tethered chains, lineage lean, migratory healing) and should be read as a conditional target and experimental record, not as the model's current established mechanism. Where its descent ontology conflicts with the volume-covering relation of Sec. 2.3, the latter takes precedence.

5.1 The mechanism: popping, voids, inflow

The mechanism that enhances popping is already implicit in the quantum bridge, but extracting it correctly requires distinguishing two rates that coincide at rest and differ in motion. The phase field of a particle is $\varphi = (Et - \mathbf{p}\cdot\mathbf{x})/\hbar$. *Along the worldline* ($\mathbf{x} = \mathbf{v}t$) it advances at $(E - pv)/\hbar = mc^2/\gamma\hbar$, the slowed internal clock, which is Eq. (18): $\chi = m/m_P$ per *processed* frame, the object's own register. *At a fixed cell of the substrate*, however, the same field advances at $\partial\varphi/\partial t = E/\hbar$, and the two rates decompose exactly:

$$\frac{E}{\hbar} = \underbrace{\frac{mc^2}{\gamma\hbar}}_{\text{worldline (register)}} + \underbrace{\frac{pv}{\hbar}}_{\text{spatial sweep}}, \tag{19}$$

the second term being the de Broglie phase gradient ($k = p/\hbar$) streaming past the cell at v. This is de Broglie's harmony of phases, realized mechanically. Now, rotation is work done against the foam's contact network, and that work is done *on cells*; the cells are the substrate and skim nothing: skimming is a property of matter moving through them, never of the foam itself. The rate the foam experiences is therefore the fixed-cell rate, counted per substrate frame:

$$\chi_E = \frac{E}{E_P} \text{ radians per substrate frame,} \tag{20}$$

reducing to m/m_P at rest, where processed and substrate frames coincide, which is why the rest case never exposes the difference. The coupling to total energy rather than rest mass is thus not an ansatz but a consequence of wave kinematics: the extra twist of a moving source is delivered to the cells by its spatial phase gradient sweeping through them. The null limit is now a corner rather than a crisis: a photon's register never advances (every frame is wholly skipped, Sec. 3.1), yet its choreography drives fixed cells at $\omega = E/\hbar$, the worldline term of (19) going to zero as the sweep term carries everything (the fixed-cell law is restated and put to further use in Sec. 7, Eq. (34), but nothing here depends on that section). A cell driven near its pressure threshold is a cell more likely to pop. One totalization note, required for the postulate to be local: the phase *rate* at a cell does not dilute with distance from the source (only the drive amplitude does), so the source strength must be weighted by where the energy resides. The coupling is therefore to the *energy density in the substrate frame*, the amplitude-weighted rotation delivered per cell per frame; its integral over a region containing the source is the enclosed energy E. We elevate this to the source law of gravitation:

Postulate 5 (Energetic source)**.** *The local enhancement of the popping rate is proportional to the phase-rotation rate delivered to the cells (the local energy density in the substrate frame, in Planck units per substrate frame, integrating to the enclosed energy over any region containing the source), with a single universal constant of proportionality for all forms of energy.*

Three consequences give the postulate its content.

The equivalence principle is structural. The coupling reads one number, the rotation budget, and is therefore blind, at fixed total energy, to composition, chemical binding, temperature, spin state, and decoherence history: thermal energy gravitates by being counted in the budget like any other energy, never read separately as temperature. Two bodies of equal energy source identical halos and fall identically, not because their differences cancel but because the foam never sees them. Eötvös-class tests, which constrain composition dependence of free fall at the 10^{-15} level, are in this reading tests of Postulate 5's single-constant clause. The same clause forecloses a tempting wrong turn: any coupling to an *activity* rate (collapse events, decoherence, interaction frequency) would make gravity depend on a body's environment at fixed energy, and a cold rock in deep space would gravitate differently from a warm one of equal total energy. It does not; gravity reads energy, not busyness.

Radiation gravitates. A photon carries $\chi_E > 0$ (by (19) its entire twist is spatial sweep, delivered at ω to every cell its choreography drives), and it therefore sources inflow like anything else. This is not optional: the expansion history of the radiation era (big-bang nucleosynthesis and the CMB acoustic structure) quantitatively requires radiation energy density to gravitate, and any source law that reads only rest mass is excluded before it leaves the page. No laboratory has yet measured the gravitational field *of* light (every classic test uses light as a falling test object, not as a source), so the sector is open experimentally; but it is not open cosmologically, and Postulate 5 passes where a matter-only coupling fails. What the postulate does *not* yet fix is how the halo of a source in motion is arranged (the sector where relativistic sources become genuinely strange), which is the subject of Sec. 5.5.

The boundary data acquire physical content. Sec. 5.3 shows that the mass must enter the flow problem as boundary data at the matter while the foam's constitutive response sets the vacuum profile. Postulate 5 says what those boundary data are: the rotation budget deposited in the foam per frame. Mass, pop size, rotation rate, and gravitational charge are one quantity, read four ways.

Remark 9 (Scope of the source law)**.** *Postulate 5 fixes the gravitoelectric sector: a coupling to energy density in the substrate frame. (That this density is foliation-dependent is not an embarrassment here, since the foliation is real in this model.) The contributions that distinguish the full stress-energy tensor from an energy density (momentum flux, pressure, the Tolman $\rho + 3p$ weighting of hot matter) are not postulated; they must* emerge *from the advection dynamics of the halo, and Sec. 5.5 states the test they must pass. The decomposition* (19) *supplies raw material for that emergence which a rest-frame scalar coupling would lack: the sweep term $pv/\hbar$ arrives with* *an intrinsic direction (the deposit is momentum-tagged), so the wake sector of Sec. 5.5 is asked to organize a directional input, not to conjure direction from a scalar. The division of labor remains deliberate: one coupling at the source, with the tensorial structure of gravitation demanded of the flow, is a stronger claim than a tensor coupling installed by hand, and correspondingly easier to falsify.*

Around any mass, cells are destroyed in excess of creation; the resulting voids are filled by lateral migration (Fig. 1), and in steady state the foam drifts inward with a velocity field $\mathbf{v}(x)$. By Sec. 2.3, "a point of space" near a mass is therefore not static: the tethered lineage chains lean inward. Space itself flows toward matter, like water toward a drain.

The tether is the ontology; the flow is its coarse grain. One misreading must be addressed. The tethered descent of Sec. 2.3 is the model's causal relation, and the cell flow is its pop-completed coarse-graining; neither, by itself, puts the gravitational warping anywhere. The warping resides in the *healing mode* of the foam, and two modes must be distinguished. If void-filling is *migratory*, neighbors under pressure expanding and sliding into the low-pressure void (both the mechanically natural behavior of a pressurized foam and what simulation shows), then volume is physically transported toward the sink, lineage chains lean inward, and the lean reproduces exactly the velocity field that flux conservation demands (verified in a one-dimensional toy, documented in Appendix C: the measured tethered-chain velocity matches the continuity prediction at the few-percent level, the tether–volume equivalence of Sec. 2.3, checked directly). If instead void-filling were *in-place*, each popped cell re-nucleated where it died, then no volume is transported, chains stand vertical, the flow vanishes, and the present section is empty; gravity would then have to fall back on the static route of the closing Remark. The model carries a physical commitment, stated plainly: *energy destroys cells faster than the void re-nucleates them locally*, so that the deficit must be supplied by transport from afar. The strength of gravity measures this destruction–replenishment imbalance (a partially in-place-healing foam rescales the effective coupling by the migrated fraction). The commitment is cheap to test: before any profile fitting, the simulation need only ask whether tethered chains around a popping-enhanced region lean. No distortion of the tiling itself should be expected; in the river formulation the slices remain flat and the cells undeformed, and the entire gravitational content lives in the lean of the chains, which is where a search for "warping" must look.

5.2 The river chronometry

Postulate 1 already measures velocity relative to the local cells, so inserting the flow yields the chronometry

$$c^2 \mathrm{d}\tau^2 \;=\; c^2 \mathrm{d}t^2 \;-\; \left|\mathrm{d}\mathbf{x} - \mathbf{v}(x)\,\mathrm{d}t\right|^2, \tag{21}$$

with *flat spatial slices, uniform cell size, and uniform tick rate*; the foam itself is unchanged near mass, only its motion changes. Equation (21) is the Painlevé–Gullstrand ("river") form of a metric, identical in structure to the acoustic metrics of analog gravity. For the radial inflow profile

$$\mathbf{v}(r) \;=\; -\sqrt{\frac{2GM}{r}}\;\hat{\mathbf{r}}, \tag{22}$$

Eq. (21) is *exactly* the Schwarzschild geometry. Three identities then hold with no further input:

1. **Free fall is advection.** A cell-comoving object accelerates at $v\,\mathrm{d}v/\mathrm{d}r = -GM/r^2$: Newtonian gravity is being carried by the river. Weight is what you feel when you refuse to go.

2. **Gravitational time dilation is kinematic.** A static observer at radius r moves at $v(r)$ *against the local substrate*, and by Eq. (7) their clock runs slow by the special-relativistic factor $\sqrt{1-v^2/c^2} = \sqrt{1-2GM/rc^2}$, the exact Schwarzschild redshift, derived as a tilt angle. There is no separate gravitational time dilation in this model; there is only one mechanism, projection, applied to motion relative to flowing cells.

3. **Light is advected.** Light moves at c relative to the flow and is carried by it, reproducing the full deflection ($1.75''$ at the solar limb), the full Shapiro delay, and the PPN parameter $\gamma = 1$, consistent with the Cassini bound $\gamma - 1 = (2.1 \pm 2.3) \times 10^{-5}$. A rate-only or conformally flat mechanism cannot do this (the former gives half the deflection, Einstein's 1911 result, and the latter none at all); the flow succeeds because Eq. (21) is not conformally flat.

An **event horizon** is the surface where the inflow reaches one cell per tick: $v = c$ at $r_s = 2GM/c^2$ (2.95 km for a solar mass). Inside, the river runs faster than light's speed through it; outgoing light makes no headway, not because anything pulls on it, but because the medium it crosses at c is itself falling faster than c. For orientation: the solar inflow is 618 $\mathrm{km\,s^{-1}}$ at the Sun's surface and 42 $\mathrm{km\,s^{-1}}$ at Earth's orbit; Earth's own inflow at its surface is 11.2 $\mathrm{km\,s^{-1}}$, the escape velocities, reinterpreted as the speeds of space.

Remark 10 (Scope of the flat-slice description)**.** *The claim that the slices stay flat, the cells undeformed, and the entire gravitational content lives in the lean of the chains is exact for a single spherical mass, and extends (with more structure, via the Doran form) to a single rotating one. It is* not *available in general: a generic mass distribution admits no globally flat spatial slicing, so the pure-river description cannot be exact for multi-body or strong-field composite systems. The weak field is safe (the halo amplitude scales as $\sqrt{M}$, the energy-like variable v^2 superposes, and the Newtonian limit is linear as required), but beyond it a residual deformation of the slices themselves must appear. The model's correction channel already exists: the position-dependent tick rate and cell size $(\varphi_\nu, \varphi_\ell)$ of the static-substrate Remark, degrees of freedom the pure river sets to zero, are exactly what a nearly-flat-slice-plus-small-deformation regime would excite. Stated as a boundary: the river is the model's exact solution for isolated bodies and its linearization elsewhere; the seam between flow and deformation is where the strong-field composite sector will be won or lost, and no claim is made about it here.*

5.3 The falsifiable target: one exponent

Everything in the preceding subsection follows from the profile (22); nothing yet derives it. That derivation reduces to a single measurable number. Newtonian gravity holds if and only if the steady-state inflow around a popping-enhanced region obeys $v \propto r^{-1/2}$, or equivalently, taking the divergence, a net cell-destruction density

$$-\nabla\cdot\mathbf{v} \;=\; \frac{3}{2}\frac{\sqrt{2GM}}{r^{3/2}} \;\propto\; r^{-3/2}, \tag{23}$$

distributed through the inflow region rather than concentrated at the mass.

The exponent has a mechanical reading that converts the curve fit into a principle. The profile $v \propto r^{-1/2}$ is precisely *ballistic inflow*: cells mobilized at rest far away and falling freely inward conserve the energy analogue

$$\tfrac{1}{2}v^2 \;=\; \frac{GM}{r}, \tag{24}$$

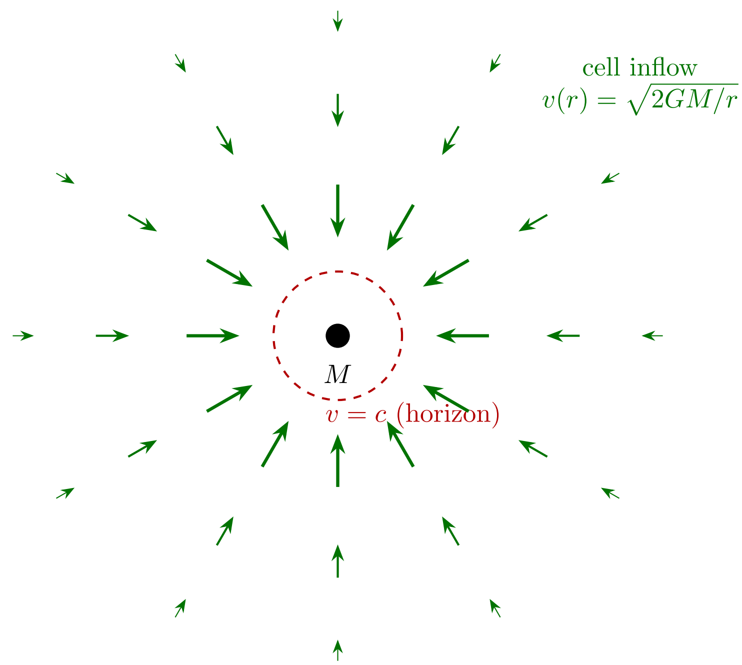

Figure 10: Gravity as cell flow. Enhanced popping at the mass consumes cells; lateral migration supplies them from outside, producing a steady inward drift with the escape-velocity profile. Free fall is comoving with the drift; static observers are swimmers holding station against it, time-dilated by their speed through the cells. The horizon is where the river reaches one cell per tick.

which is Eq. (22) rearranged: the river runs at escape speed because escape speed is what free fall from rest at infinity delivers. The distributed sink (23) is then not an independent assumption but the consistency condition: the shell flux $4\pi n_0 r^2 v \propto r^{3/2}$ *grows* outward, so inflow that is ballistic must also be consumed en route at exactly the $r^{-3/2}$ halo rate, or the flux books do not balance. One statement , *the foam falls freely and is eaten as it falls*, fixes both the velocity profile and the destruction halo. For the simulation program this upgrades the question. Rather than fitting a power law and hoping the exponent is stable, the rig can test the principle directly: measure whether the relaxed inflow satisfies the free-fall relation (24) locally (acceleration equal to $v\, \mathrm{d}v/\mathrm{d}r$ with no residual constitutive force in the bulk), and whether the measured consumption density matches the divergence of the measured flow. A relaxation law that passes both is not merely consistent with Newton; it explains *why* the exponent is $-1/2$ (the halo does no work on the falling cells), and a law that produces $-1/2$ while failing the local free-fall check is a coincidence to be distrusted.

The exponent is the entire game, and it discriminates sharply between constitutive behaviors of the foam: an incompressible point sink gives $v \propto r^{-2}$ (gravitational acceleration falling as $1/r^4$, excluded); a diffusive closure $\mathbf{J} \propto -\nabla n$ with a localized sink gives the same r^{-2} and is likewise excluded. The foam must do something subtler: the destruction must be distributed as (23). The simulation task is direct: introduce a localized popping enhancement, let void-filling relax to steady state, and fit the inflow profile to a power law. A robust, parameter-stable exponent of $-1/2$ would constitute a derivation of the inverse-square law from cell microphysics; any other exponent falsifies the mechanism as stated and identifies exactly what constitutive ingredient is missing. One further robustness demand is recorded here, ahead of results to be reported separately. A candidate microphysics for Postulate 5 has the drive *suppressing* the popping of the cells it occupies: a driven (spinning) cell resists destruction, and the pop burden it sheds is displaced by crowding onto its immediate neighbors, realizing the distributed enhancement one cell layer out rather than in place. Under that mechanism the source is a protected core wrapped in a destruction shell, and the exponent target inherits an additional clause: $v \propto r^{-1/2}$ must *survive the enhanced survival of driven cells at the core.* A steady-state inflow measured around such a protected core that departs from $-1/2$ falsifies that microphysics without touching the ladder above it.

Preliminary local-relaxation test. A separate local-relaxation simulation probes the same target without prescribing the halo profile. The code removes particles near a central source, reintroduces replacements at the outer boundary, and lets local packing forces move the remaining particles. Long runs measure a net radial material velocity near $v(r) \propto r^{-1/2}$. The result remains provisional: the velocity fit has low R^2, the density profile is noisy, and the default cohesion law is a constitutive choice. The test gives an encouraging existence hint. A derivation requires parameter sweeps, random seeds, larger particle counts, and alternative local relaxation laws.

The certified-medium campaign: a negative result for the flow route. A pre-registered gate sequence hardened the three-dimensional rig into a “certified medium”: sliding local capacity at one cell per Planck volume, migration-first step order, and a quantile popping threshold with no runtime population feedback. The medium passed its stability gates (bounded occupancy under drive at $\kappa = 1$, $\rho \in \{0.35, 0.5\}$, 250 frames, exact identity-level cell accounting) and its healing-speed gate (a force-emptied cavity of $r < 2$ spacings refills to ambient within two frames). A pre-registered single-seed calibration then measured the drain response; the measured null put the six-seed gate criterion out of reach, and the campaign stopped at its no-flow condition rather than run the gate. Under a sustained sink of 11 cells per frame within $r \leq 3$ spacings (24^3 target cells, 250 frames, paired baseline), the foam holds a shallow occupancy deficit confined to the drain region: 12–16% in shells 0–2, 1.4% in shell 3, zero beyond. It drives no measurable radial flux. Clean-window shell velocities read $|v| \leq 0.006$ spacings per frame with mixed signs; continuity predicts 0.012–0.029 for the imposed consumption. The same lean instrument reads imposed uniform advection correctly in the kinematic shift gates, so the null belongs to the medium and not to the readout. The mechanism is identifiable: threshold popping calibrated on crowding acts as a local density-restoring force. A sink lowers crowding where it bites, fewer candidates pop there, and the deficit refills in place. Deleting the global population feedback did not delete this response, because the response lives in the local crowding dependence itself; the medium realizes the demand-elastic creation its constitutive rules were written to exclude. The cavity gate agrees: refill arrives within one to two frames by local nucleation, with no donor deficit in the surrounding shells. Healing in this constitutive family is in-place, not migratory. That fires the gravity-engine row of Table 1 and falsifies the flow route for this family. The chronometry theorem does not depend on the flow sector; the river kinematics of Sec. 5 remain an exact correspondence awaiting a medium that produces the profile; the weak-field burden now rests on the static-substrate alternative (the closing Remark of Sec. 5.4) or on a different constitutive family under a fresh pre-registration ledger.

The retardation campaign: a negative result for the static route. A second pre-registered ledger gave the static-substrate Remark its first cell-level candidate: mass *retards* nucleation. The hypothesis holds that a source suppresses cavitation in its neighborhood, the suppression propagates outward along the descendant tree, and the accumulated differential realizes the two static fields directly, a slower tick rate φ_ν where turnover falls and a denser foam φ_ℓ where survivors accumulate. The transducer half of this hypothesis passed its existence test. A 50% nucleation veto within $r \leq 3$ spacings of the source, imposed on the same certified medium, settles into a stable equilibrium with per-cell turnover at $0.489\times$ baseline and committed occupancy at $1.354\times$ baseline, three seeds agreeing to three significant figures. This is the program's first intervention that moves both metric dials at once with both signs correct: a slower local clock, and excess cells near mass (the excess-radius signature). The carrier gates bracketed what conducts the effect outward. Occupancy and internal pressure both screen within $\lambda \approx 2$ spacings and transmit the remainder as a gradientless global offset, so neither can hold a $1/r$ profile; a conserved tree-borne field diffuses at $D \approx 0.11$ spacings^2/frame toward the clamped $1/r$ harmonic, with its steady state unconfirmed at the affordable run length.

The gravity verdict then reduces to one ratio. The static route requires $\varphi_\ell = \varphi_\nu$, which in cell-count terms reads $\delta n/n = -3\,\delta\nu/\nu$: three units of space response per unit of tick response, $\eta_0 = 3$. A pre-registered rate sweep (retardation strengths 0.05 to 0.5 against a common baseline) measured both responses individually near-linear and their ratio flat, η between 0.566 and 0.703 across the tenfold range, with weighted intercept

$$\eta_0 \;=\; 0.605 \pm 0.058.$$

The corresponding solar-limb deflection, $0.876''\,(1 + \eta_0/3) = 1.053'' \pm 0.017''$, sits roughly forty standard errors below the observed $1.752''$, and the flatness of η(rate) forecloses rescue by extrapolation: the lowest-rate point alone excludes the survival band at ten standard errors. The pre-registered kill condition fired on 2026-07-20. The mechanism is again identifiable, and it is the same regulator that answered the drain. The veto suppresses turnover one-for-one, but occupancy rises only until the quantile threshold restores candidate crowding, and that restoring response caps the space dial at two-thirds of the tick dial, a fifth of the requirement. Within this constitutive family, density fails as the spatial half of the metric on both counts: it cannot hold the $1/r$ shape (screened) and it cannot reach the required amplitude (ratio 0.6 for 3). The retardation route joins the flow route as falsified. What survives the two campaigns: the chronometry theorem, which depends on neither; the two-dial transducer as a measured medium property; and the conserved tree-borne field as the only unscreened long-range channel any probe has found. What any successor mechanism now owes, on the record: a spatial carrier that is neither density nor pressure, a space response three times the tick response in the linear limit, survival against the crowding regulator that erased both predecessors, and the axial field of Sec. 5.5.

The destruction halo. The required sink's structure reshapes what "matter enhances popping" means. Decompose any steady spherical flow as $v(r) = Q/(4\pi n_0 r^2) +$ (halo response): a point sink Q at the matter contributes an r^{-2} profile. The Painlevé–Gullstrand profile contains *no* r^{-2} component, so $Q = \lim_{r\to 0} 4\pi n_0 r^2 v = 0$ identically: *the point destruction at the matter is exactly zero, and all destruction is distributed through the surrounding halo* as Eq. (23). Matter does not eat space; it *conditions* the surrounding foam to pop, the cell-level analogue of mass being boundary data for a vacuum field in general relativity. Two consequences follow. First, the halo amplitude scales as $\sqrt{M}$ (cumulative destruction inside r is $4\pi n_0 \sqrt{2GM}\, r^{3/2}$), so inflow speeds of neighboring masses do not superpose, but v^2, the energy-like variable, does, exactly as the linear Newtonian limit requires. Second, the halo cannot extend indefinitely (its integrated destruction grows as $r^{3/2}$); it terminates where the gravitational inflow hands over to the cosmological outflow of net creation (Sec. 6), at $r_t = (2GM/H^2)^{1/3}$: 121 pc for the Sun, 1.2 Mpc for a Milky-Way-mass galaxy, 12 Mpc for a rich cluster, the turnaround scales of standard structure formation. The destruction halo is a finite, bounded *deficit against the universal creation budget*: gravity and expansion are the two signs of one ledger. The seam at r_t, however, is a crossover of flow direction, *not* a local balance of that ledger, and honesty requires the imbalance to be stated: integrating (23) to r_t gives a cumulative destruction $4\pi n_0(2GM)/H$, while the creation budget inside the same radius is $\frac{4}{3}\pi n_0(2GM)/H$: the halo consumes exactly *three times* what is created within its own turnaround surface. A gravitationally bound region is a net consumer, funded from beyond r_t, which is one microscopic face of matter back-reaction on the expansion rate (Sec. 6); and near r_t itself the sink density is properly the divergence of the *net* flow, inflow plus the $+3H$ creation term, a matching problem the pure gravitational profile above does not solve. The seam is a target, not a result. For the derivation program this sharpens the target: a *local* power-law closure $P_{\text{net}} \propto -v^n$ can fix the exponent (e.g. $n = 3$ yields $p = -1/2$) but pins the amplitude universally, with no memory of M; the mass must enter through boundary data at the matter while the foam's constitutive response sets the vacuum profile, the same division of labor as in field theory, now demanded of the foam.

5.4 The constitutive ladder for the Newtonian profile

This subsection reorganizes the constitutive discussion into a ladder whose load-bearing rung is explicit. The weak-field content of the mechanism (the $1/r$ potential, the $r^{-1/2}$ inflow, the $r^{-3/2}$ destruction halo, the universality and constancy of G, and the superposition law) follows from the postulates already on the ledger plus one new one (comoving exit, Lemma 5.4.4), with a single dimensionless calibration condition left over. In particular the destruction halo is not assumed anywhere below: it emerges in Lemma 5.4.3 as bookkeeping. Throughout, $\delta P(r)$ denotes the pressure deficit (the amount by which the foam's ambient squeeze is relieved at radius r from a source), and ρ the foam's inertial density.

Standing postulates used below

1. *Energetic source.* Matter pops cells at its own location at a rate proportional to the phase rotation it delivers to the cells per substrate frame (its energy density in the substrate frame, integrating to $\chi_E = E/E_P$), with one universal constant for all forms of energy (Postulate 5).

2. *Saturation.* The vacuum holds one cell per Planck volume and cannot compress: any convergent flow must destroy cells at exactly the local compression rate.

3. *Migratory (cross-frame) healing.* A cell's motion is carried across frames (geometrically, the lean of its lineage chain) and is edited, not set, by the force acting on it.

5.4.1 Lemma 1: the pressure deficit is harmonic

Lemma 1 (Harmonic deficit)**.** *In steady state, outside all sources, the pressure deficit satisfies* $\nabla^2 \delta P = 0$*; around an isolated source it therefore takes the form*

$$\delta P(r) \; = \; \frac{A}{r}, \tag{25}$$

with amplitude A fixed by boundary data at the matter.

Mechanism. A cell whose neighbors are unequally squeezed is pushed toward the softer side and shifts (lateral shift within a forming frame, voids filled as they open) until the squeeze it feels balances. Balance for an evenly surrounded cell means its own squeeze equals the average of its neighbors'; equality-with-the- neighbor-average is precisely the discrete Laplace condition, so the equilibrium field is harmonic wherever no volume is being created or destroyed out of balance. In three dimensions the influence of a central source must cross every enclosing sphere undiminished while the spheres' areas grow as r^2; the gradient therefore falls as r^{-2} and the deficit as $1/r$. Two scope notes. First, the endpoint is a *steady state*, not flatness: with the source consuming continuously, (25) is the one profile at which the healing inflow delivers volume exactly as fast as it is consumed, the standing deficit continuously regenerated, as in the static-field discussion elsewhere in this paper. Second, the field is treated as quasi-static, valid when the flow is slow against the foam's signal speed ($v \ll c$); the derivation is expected to bend in the near-horizon regime, where general relativity bends likewise.

5.4.2 Lemma 2: ballistic response selects the exponent

Lemma 2 (Ballistic profile)**.** *A drag-free cell mobilized essentially at rest far from the source and falling in the field* (25) *satisfies the work–energy relation*

$$\tfrac{1}{2}\rho\, v^2(r) \;=\; \int_r^\infty \frac{A}{r'^2}\,dr' \;=\; \frac{A}{r}, \qquad \textit{hence} \qquad v(r) = B\,r^{-1/2}, \quad B^2 = \frac{2A}{\rho}. \tag{26}$$

The steepness of the $1/r$ deficit is an inverse-square force per volume, A/r^2; this is the origin of the inverse-square law in the model. What converts an r^{-2} *force* into an $r^{-1/2}$ *speed* is memory: under migratory healing each frame's push adds to the speed already banked, and the integral in (26) is that accumulation. The alternative (in-place healing, speed proportional to force) yields $v \propto r^{-2}$, the Darcy branch, excluded by the Newtonian limit. The branch choice is therefore not a tunable: postulate (3) *is* the claim that the foam is on the ballistic branch, and the measured force law is its test. Starting the fall from rest at the turnaround radius r_t (Corollary 2) rather than infinity multiplies (26) by $(1 - r/r_t)$; at 1 AU around the Sun this is a correction of 4×10^{-8}. Calibrating $A/\rho = GM$ (Lemma 5.4.5) gives $v = \sqrt{2GM/r}$; numerically, 42.13 km/s at 1 AU, the solar escape speed, and the local acceleration $v\,dv/dr = -GM/r^2$ follows by differentiation.

Remark 11 (Where the ladder's weight actually sits)**.** *Lemmas 5.4.1 and 5.4.2 are not independent rungs, and it would misrepresent the ladder to count them as two. For any drag-free radial flow from rest at infinity, the force-free momentum balance of Lemma 5.4.4 integrates to $\delta P = \frac{1}{2}\rho v^2$ (Bernoulli) for* every *profile; given ballistic response, "δP is harmonic" and "$v \propto r^{-1/2}$" are one statement in two variables. All of the physics therefore concentrates in Lemma 5.4.1, and its mechanism paragraph must carry a tension it should not hide: the neighbor-average argument is quasi-static,* relaxational *reasoning (cells shifting until squeeze balances), while Lemma 5.4.2 requires the same cells to be* drag-free*, banking velocity across frames rather than equilibrating. Stated as a single constitutive demand, the foam is being asked to be four things at once: a Laplace equilibrium medium (in pressure), an Euler fluid (in momentum), incompressible (at saturation), and a ballistic transport medium (across frames). That is the constitution of a perfect fluid, which is a consistent thing to be, but it is one assumption wearing four names, not independent derivations. This is the precise content of the "load-bearing assumption" recorded in the claim status below, and it is why the simulation program's pressure probe measures harmonicity rather than assuming it: a foam whose microdynamics delivers the* *neighbor-average equilibrium* and *the drag-free fall is exactly what the rigs must exhibit, not what this ladder can grant itself.*

5.4.3 Lemma 3: the destruction halo is bookkeeping

Lemma 3 (Emergent halo)**.** *Under saturation, the ballistic inflow* (26) *forces distributed cell destruction at the volumetric rate*

$$S(r) \;=\; \rho\,\big|\nabla\!\cdot\mathbf{v}\big| \;=\; \frac{3}{2}\,\rho B\,r^{-3/2}. \tag{27}$$

Conversely, the point-sink profile $v \propto r^{-2}$ is exactly divergence-free and forces no bulk destruction.

Nothing about an $r^{-3/2}$ halo is assumed: (27) is the divergence of (26), i.e. the exhaust of a convergent flow through a foam that cannot compress. Both branches of Lemma 5.4.2 satisfy saturated continuity (r^{-2} with no halo, $r^{-1/2}$ with the emergent halo), so the halo's existence and shape stand or fall with the ballistic branch, and the two observables (inflow exponent; presence and shape of distributed destruction) are a matched pair for any future numerical test.

5.4.4 Lemma 4: the exhaust does not dent the field

Lemma 5.4.1 assumed no unbalanced volume change outside the matter; Lemma 5.4.3 then filled that region with pops. Neutrality must therefore be shown, in three parts.

Lemma 4 (Neutrality of stimulated pops)**.** *The halo destruction* (27) *contributes no source term to the equation of Lemma 5.4.1 and no force term to the relation of Lemma 5.4.2, provided popped cells exit comoving (postulated below).*

(i) Volume. A source term arises only from *imbalance*: volume destroyed minus volume delivered by the flow. The matter is a genuine source because χ_E consumption proceeds regardless of delivery. A compression pop, by contrast, fires when and because the flow has over-delivered one cell volume, and removes exactly that volume: trigger equals excess, removal equals trigger. A sink slaved to the flow cannot source the field the flow answers to; the right-hand side of the Poisson equation is confined to the matter and to the spontaneous channel (Corollary 3).

(ii) Graininess. Pops are discrete; each is a one-cell dent healed in roughly one frame. The fraction of foam mid-transient at any instant is (rate per cell)×(healing time) $\approx \frac{3}{2}(v/c)(\ell_P/r)$: about 2×10^{-50} at 1 AU around the Sun, and still only $\sim 8 \times 10^{-39}$ at the solar Schwarzschild radius where $v \to c$. The exhaust is a continuum for all purposes.

(iii) Momentum. Popped cells are moving cells. For a flow with a mass sink of rate density σ whose removed material exits at velocity u, the surviving cells obey

$$\rho\,(\mathbf{v}\!\cdot\!\nabla)\mathbf{v} \;=\; -\nabla P \;-\; \sigma\,(\mathbf{u}-\mathbf{v}), \tag{28}$$

so the sink is force-free if and only if $\mathbf{u} = \mathbf{v}$: the removed cell takes its own momentum out of the books (the rocket equation run backward: mass leaving at the local velocity exerts no thrust on what remains). We therefore adopt:

Postulate 6 (Comoving exit)**.** *A pop removes the cell and its motion together. Momentum is cell-state (the lean of the lineage chain) and is deleted with the chain; nothing is bequeathed to the neighbors.*

Two corollaries come free. The popped cell's kinetic energy exits with it, which is precisely the no-heating condition a steady halo requires. And in the vertex-nucleation ontology (Remark 13) the postulate costs nothing: motion there is a pattern of succession, not a substance, and a terminated lineage trivially bequeaths nothing. Internal consistency check: had momentum instead been handed to neighbors ($\mathbf{u} = 0$), (28) adds an inward body force throughout the halo, Bernoulli breaks, and the escape-speed calibration of Lemma 5.4.2 fails; it does not fail.

5.4.5 Lemma 5: calibration, universality, superposition

Lemma 5 (Calibration)**.** *Write the source pop rate as $\lambda\,\chi_E$ per frame and the foam's deficit response as $\delta P = \kappa\,\rho\,Q/(4\pi t_P r)$ for unbalanced volume consumption Q, with λ, κ dimensionless microphysical constants. Then for rest energy $E = Mc^2$,*

$$G \;=\; \frac{\kappa\lambda}{4\pi}\,\frac{c^2\,\ell_P^3}{E_P\,t_P^2}, \qquad \textit{and identically} \qquad \frac{c^2\,\ell_P^3}{E_P\,t_P^2} \;=\; G, \tag{29}$$

so the entire calibration reduces to the single condition $\boxed{\kappa\lambda = 4\pi}$.

Three consequences, each carrying its own falsifier. *(a) Universality.* M cancels in (29) only because the source coupling is linear in E; any nonlinearity makes the effective G mass-dependent, a Nordtvedt-type violation tightly bounded by lunar laser ranging. *(b) Constancy.* κ is a constitutive constant of the foam; secular drift in the foam's state would appear as $\dot{G} \neq 0$, bounded observationally near $|\dot{G}/G| \lesssim 10^{-13}\,\mathrm{yr}^{-1}$. *(c) Scale.* The model cannot predict the value of G without deriving κ and λ, and the second equality in (29) should be read for what it is: an *identity by construction*, since ℓ_P, t_P, and E_P are themselves defined from G. That the combination lands on G is not a result of the model; the sole content of the calibration is the reduction of two microphysical constants to the single condition $\kappa\lambda = 4\pi$ (a Gauss-shell factor, plausibly a derivable statement about influence spreading over spheres rather than an empirical input), and even that is a reparametrization until κ or λ is computed independently from cell mechanics.

Superposition. The field equation of Lemma 5.4.1 is linear with sources on the right-hand side, so amplitudes stack: $\delta P = \sum_i A_i/r_i$. Through $B^2 = 2A/\rho$ it is therefore v^2 that superposes, not v (energies add, speeds do not), reproducing the linearity of the Newtonian potential; the $\sqrt{M}$ scaling of B is the shadow of the square root in the work–energy relation, not a failure of superposition. One caveat must be carried openly rather than in a parenthesis. Pointwise addition of v^2 cannot describe a vector sum of flows ($|\mathbf{v}_1 + \mathbf{v}_2|^2$ contains the cross term $2\mathbf{v}_1\cdot\mathbf{v}_2$), so the multi-source flow field is *not* the sum of single-source fields. What superposes exactly is the scalar deficit; the speed magnitude then follows from Bernoulli along streamlines from rest, and the streamline geometry, the continuity equation, and the required sink distribution must be solved *jointly* for multiple sources. That joint problem is unsolved; the claim here is limited to the scalar sector in the weak field, where the Newtonian potential is recovered through δP, and the strong-field composite case is bounded by the flat-slice scope remark elsewhere in this paper.

5.4.6 Corollaries and remarks

Corollary 2 (Turnaround radius)**.** *Inflow $\sqrt{2GM/r}$ and creation-driven outflow Hr cancel at*

$$r_t = \left(\frac{2GM}{H^2}\right)^{1/3}: \tag{30}$$

$\sim$121 *pc for the Sun,* $\sim$1.2 *Mpc for a Milky Way–mass system, the latter roughly where the Local Group in fact decouples from the Hubble flow. Two qualifications keep this honest. First, the agreement is dimensional consistency, not corroboration: any theory containing* G*,* M*, and* H *possesses this scale, and standard cosmology places its zero-velocity surface at the same order. Second,* r_t *marks where the flows cancel, not where the books balance: the halo consumes three times the creation budget inside* r_t *(Sec. 5.3), so the crossover is a seam still owed a matching calculation.*

Corollary 3 (Two pop channels)**.** *Destruction runs in two channels. The* stimulated *channel is slaved to the flow (Lemma 5.4.3); per cell it runs at* $\frac{3}{2}v/r$ *and constitutes gravity. The* spontaneous *channel is the popping of the creation excess in regions with no drain; per cell it runs at* $\varepsilon/t_P = H$ *(numerically* $2.2 \times 10^{-18}\,\mathrm{s}^{-1}$*, an identity: the excess rate* is *the Hubble rate) and is identified with vacuum fluctuation phenomenology. The channels equalize at* $r = (3/2)^{2/3} r_t \approx 1.31\, r_t$*, the same boundary, within an order-one factor, that separates inflow from outflow. Inside a well the stimulated channel dominates by* $\sim 2 \times 10^{11}$ *at* 1 *AU; locally minted excess is absorbed by the flow (absorption time* $\sim$ *weeks against a spontaneous fuse of* $\sim 1/H \approx 14$ *Gyr), so spontaneous popping is suppressed in wells, graded with potential, vanishing at* r_t*. Open fork, on the ledger: whether vacuum-fluctuation phenomenology tracks the* net *excess channel (rate* H*; graded suppression in wells, in principle constrained by null gravitational-redshift experiments) or the* gross *nucleation attrition of Remark 13 (rate* $\sim$1 *per cell per frame; well modulation a part in* 10^{50}*, unobservable). The choice changes the testability of the suppression claim and must be made explicitly.*

Remark 12 (Momentum as lineage lean)**.** *Momentum in this model is inter-frame geometry: the lean of the lineage chain, inherited by default (Newton's first law) and edited by pressure imbalance (the second). It cannot exist within a single frame (a lean is a relation between frames), so migratory healing is not merely permitted but required: a model of complete per-frame snapshots has nowhere to store momentum. The causal speed is the maximal lean, one cell diameter per frame; the* 1 *AU solar inflow is a lean of* 1.4×10^{-4} *diameters per frame. The ambient pressure gradient is* not *momentum but force: identifying the two is the Aristotelian error and reproduces the excluded Darcy branch; a moving cell's material signature is instead a bound, cell-scale fore-aft pressure asymmetry carried with the chain, which the ambient gradient increments each frame.*

Remark 13 (Vertex nucleation)**.** *The lean requires descendants positionally distinct from parents; vertex nucleation supplies this natively (motion = persistent bias in the succession direction; rest = balanced succession;* c *= one vertex hop per frame, so the speed limit is nucleation geometry rather than a postulate) and makes Postulate 6 automatic. The gross bookkeeping must be stated carefully. Under Poisson–Voronoi statistics the foam mints* $\simeq 6.8$ *candidates per surviving cell per frame (Sec. 7.2), so the survival fraction of candidates is* $\simeq 1/6.8 \approx 0.15$*, overwhelmingly as* replacement*. The net excess* $\varepsilon \approx 1.2 \times 10^{-61}$ *per frame is not a survival fraction but the excess-above-replacement fraction of candidates,* $\varepsilon/6.8 \sim 2 \times 10^{-62}$*: of every* $\sim$7 *candidates, one survives, and the survivor is new growth rather than replacement once in* $\sim 10^{61}$ *frames per cell. The attrition itself (*$\simeq 5.8$ *pops per surviving cell per frame) is the natural identity for the* gross *branch of the fork recorded in Corollary 3.*

Remark 14 (Shared propagation speed; electromagnetic constants)**.** *Everything the substrate carries propagates by frame-hops, so the speed of gravitational signals equals the speed of light by construction; in a two-medium world this equality could fail, and it is measured to hold to* $\sim 10^{-15}$ *(GW170817). For the same reason* $\epsilon_0 \mu_0 = 1/c^2$ *is not a law to derive but the statement that light* *rides the substrate. Structurally, κ and λ are the compression sector's compliance and source coupling, as ϵ_0 and the charge quantum are the rotation sector's; the contrast is that gravity's dimensionless product is geometric ($\kappa\lambda = 4\pi$, the medium-constant form of the equivalence principle) while electromagnetism's is not ($\alpha = 1/137.04$). Deriving the rotation-sector constants, and with them α and the 4×10^{42} electron force ratio, is relocated by this model from "law of nature" to "material property of the foam": a marked door, explicitly not a claimed result.*

Claim status

Derived here, conditional on the standing postulates: the $1/r$ potential, inverse-square force, $r^{-1/2}$ inflow, $r^{-3/2}$ emergent halo, force-free exhaust, universality and constancy of G, superposition of the scalar deficit (with the vector flow problem open), turnaround radius, channel structure. (The "Planckian scale of G" is deliberately absent from this list: it is an identity of Planck units, not a result; see Lemma 5.4.5.) Newly postulated: comoving exit (Postulate 6; free under vertex nucleation). Left open, on the ledger: the value of $\kappa\lambda$ beyond the calibration 4π; the spontaneous-channel identification fork; the multi-source streamline problem; and the harmonicity of δP under the model's own microdynamics, which, per Remark 11, is where essentially the entire weight of the ladder sits, the load-bearing assumption this ladder converts from implicit to explicit and which the simulation program's pressure probe is designed to measure rather than assume.

Remark 15 (Static-substrate alternative)**.** *If the flow contribution were absent, the same observations could be carried instead by inhomogeneous substrate properties: a position- dependent tick rate* $\nu = t_P^{-1}(1+\varphi_\nu)$ *and cell size* $\ell = \ell_P(1+\varphi_\ell)$*. Redshift experiments fix* $\varphi_\nu = \Phi/c^2$*; light propagation (deflection, Shapiro) fixes* $\varphi_\nu + \varphi_\ell = 2\Phi/c^2$*; together* $\varphi_\nu = \varphi_\ell = \Phi/c^2$*. The two routes realize the same geometry in different slicings and are classically indistinguishable; tethered descent selects the flow picture, since the comoving congruence is physically defined by the lineage of the cells themselves. In either route a local observer counts cells per tick and measures the speed of light to be exactly c, so local Lorentz invariance is automatic rather than imposed. The retardation campaign of Sec. 5.3 gave this route its first cell-level candidate and measured the ratio:* $\varphi_\ell/\varphi_\nu = \eta_0/3 = 0.202 \pm 0.019$ *against the required* 1*. The certified family delivers a fifth of the spatial response the deflection data demand.*

5.5 Moving and null sources: the second target

Everything so far concerns a static mass. The halo of Sec. 5.3 was solved as a time-independent boundary problem, and nothing yet says what the foam does around a source in motion. This is not a corner case to be deferred politely: the null limit is where general relativity's answer is sharp, strange, and already known, so it functions as a second falsifiable target for the flow dynamics, on the same footing as the inflow exponent.

The known answer first. In general relativity the source of gravity is the full stress-energy tensor, and for null sources this has a qualitative signature, worked out by Tolman, Ehrenfest, and Podolsky in 1931: two parallel light beams propagating in the *same* direction exert no gravitational attraction on each other, while antiparallel beams attract with *twice* the strength naively estimated from their energy alone. The same doubling is the second half of the $1.75''$ solar deflection; both trace to the null character of the participants. A theory that couples gravity to energy density alone, with no velocity structure, gets this wrong in both directions: it predicts parallel beams attract and antiparallel beams attract no more strongly. The velocity structure of the source is therefore not decoration; it is load-bearing, and it is measured (indirectly but quantitatively) every time the full deflection and Shapiro delay are confirmed.

What the foam must do. Postulate 5 deposits rotation budget wherever the energy is; for a moving source the deposition region moves, and the destruction halo cannot remain the static solution of Sec. 5.3: it must be *advected with its source*, trailing a wake in the cell flow. That wake is where the missing tensor structure has to live: in the linearized regime the flow field $\mathbf{v}$ splits into the potential inflow of the static problem (gravitoelectric) and the rotational/wake component sourced by momentum flux (gravitomagnetic), and the demand is that the covariant flow dynamics of the roadmap deliver both from the one scalar coupling plus advection. The pass/fail condition is then concrete:

> *In the null limit, the wake of a source region translating at c must exert zero transverse drag on co-moving null trajectories, and enhanced (doubled) drag on counter-propagating ones.*

Pass, and the model owes nothing further to the classic tests: the factor of two in the deflection was already banked in Sec. 5, and Tolman–Ehrenfest–Podolsky comes with it. Fail, whether by a wake that attracts co-moving light or one whose counter-propagating pull is unenhanced, and the mechanism is excluded by the same solar-limb measurement that killed the rate-only route, however well the static exponent behaves. The condition also disciplines the constitutive search: many relaxation laws that produce a static $r^{-1/2}$ halo will presumably differ in their wakes, and the null-limit condition is the knife that cuts between them.

A simulation form of the test exists, well downstream of the exponent program but stated now so the target is on the ledger: translate a popping-enhancement region through the relaxed foam at a controlled speed, and measure the transverse drift induced in tracer descendant chains co-moving with, and counter-propagating against, the source. The static rig of Sec. 5.3 measures one exponent; this rig measures one asymmetry. Between them they bracket the entire weak-field content of the mechanism.

Two further consequences ride along. First, a wake sourced by momentum flux is frame dragging: the Kerr sector, and with it the Gravity Probe B and LAGEOS constraints, become downstream checks of the same advection structure rather than separate postulates. Second, the Tolman weighting of hot matter ($\rho + 3p$) must emerge when the wakes of a source's internal constituents are averaged (a box of photon gas is, microscopically, a superposition of null wakes), so the remark closing Sec. 5.3's source law acquires its test here too. None of this is derived; all of it is now demanded, which is the paper's preferred relationship with its open problems.

The two negative results of Sec. 5.3 raise the stakes in this sector. The falsified river carried the model's only representation of the Kerr cross term $g_{t\varphi}$: frame dragging is odd under time reversal, and no scalar substrate field (tick rate, cell count, cell size) can build it. Schwarzschild tolerates a scalar substrate; Kerr does not, and every astrophysical black hole with a measured spin is a Kerr source. A successor mechanism therefore owes this sector an axial, handed substrate field: a standing chiral pattern in nucleation preference, in tether-forest orientation, or in the conserved carrier of Sec. 5.3, biased by the momentum-tagged sweep of (19). Whether the medium's regulators erase such a field admits the same cheap pre-registered test pattern as the completed campaigns: impose an azimuthal nucleation bias, then measure its persistence and range.

6 Cosmology: two modes of expansion

The two-mode picture of Fig. 2 frames the cosmology. Gravitation and cosmic expansion are the same object in this model, the divergence of the cell flow, with opposite signs: local net destruction makes space converge (gravity, Sec. 5), global net creation makes it recede from itself (expansion).

This section states what the two-mode picture supplies and, at greater length, what it does not. It contains no cosmological prediction. One earlier variant of the model is falsified here and recorded; one mechanism proposed for primordial perturbations is falsified here and recorded. What survives is an ontology with a single measurable entry point.

Mode 1 addresses the horizon problem, without a clock. The deepest puzzle inflation was invented to solve is the horizon problem: regions of today's sky that light could never have connected share the same temperature to one part in 10^5. In the clockless lateral mode there is no speed (including c) defined in Mode 1, because speed requires metric duration. The speed of light is a property of frames (one cell per tick), and mode 1 has no frames. But the claim must be phrased in the vocabulary mode 1 actually possesses (Sec. 2.2): generation order, not duration. No *equilibration* is available in a clockless phase, since equilibration is dynamics, so the uniformity cannot be established by any process; it must be a *structural property of the packing statistics*, homogeneous by construction across the growing foam and inherited by the frame era at saturation. That the nucleation statistics deliver homogeneity to at least one part in 10^5 is therefore a requirement of this mechanism, measurable in simulation alongside $S(k)$ below, not a consequence to be pocketed. Note the distinction from standard inflation, which is rapid expansion *in time*: mode 1 is pre-temporal, closer to signature-change and no-boundary proposals in which time emerges from a timeless regime, but with a concrete mechanism (pressure saturation) rather than a boundary condition. The onset of time is non-singular: the first frame is a layer of cells, preceded by mode-1 succession without metric duration, not by infinite density.

Two limits bound the claim, and the second is severe enough to be stated as a remark at the end of this section. First, inflation does more than solve the horizon problem: it dynamically flattens, and it generates adiabatic, phase-coherent perturbations whose signature the CMB acoustic peaks confirm. Mode 1 addresses the horizon problem only, flatness here being a property of the mode-2 patch that is assumed consistent rather than driven. Second, and worse, the mechanism that must deliver homogeneity is the same mechanism that was asked to deliver inhomogeneity, and it cannot do both.

Flatness, and a recorded falsification. An earlier variant of this model took the universe to be the literal boundary 3-sphere of a closed four-dimensional ball of radius $R = ct$. That variant fails, and the reason matters: a 3-sphere of curvature radius ct_0 predicts spatial curvature $\Omega_k = -(1/H_0t_0)^2 \approx -1.1$, while CMB and BAO measurements give $\Omega_k = 0.0007 \pm 0.0019$, a discrepancy of roughly 580σ, by direct measurement of angular scales rather than by model preference. The two-mode picture passes where the closed variant fails: the visible universe is a patch deep inside the flat frame-producing region, with whatever global structure exists (the mode-1 rim) beyond the horizon. The closed variant's one attractive by-product, the parameter-free prediction $H = 1/t$, is lost with it, and nothing here replaces it.

The expansion rate: the model has no expansion dynamics. Within the saturated region, nucleation continues: each new frame carries slightly more cells than its predecessor, the excess being the lateral creation that pressure could not suppress. If the per-frame fractional *linear-scale* excess is ε, the Hubble rate is $H = \varepsilon/t_P$, and the measured H_0 corresponds to $\varepsilon \simeq 1.2 \times 10^{-61}$ per frame; since $V \propto a^3$, the corresponding fractional excess in cell count is 3ε to first order. This is a translation of the measured H_0 into Planck units, not a prediction; nothing in the model currently constrains ε.

Worse, no dynamical law is available to evolve it. A constant microphysical imbalance gives constant H: de Sitter expansion for all time, with no radiation era and no matter era. There is no Friedmann relation $H^2 \propto \rho$ in the two-mode picture, and it is not merely underived — the model's own signs run the wrong way for the naive repair. Matter's cell consumption (Sec. 5) *subtracts* from net creation, so a higher matter density in the past would give a *lower* H in the past, where observation requires $H(z \simeq 1100) \approx 2 \times 10^4 H_0$ and vastly more at nucleosynthesis. Any successor account must therefore supply an expansion history that was fast and decelerating, from a mechanism in which matter does not simply suppress creation. Supplying it is roadmap item 2; until it is supplied, this model has a cosmological ontology and no cosmology.

Two further items are open at the same level. Uniform insertion everywhere plausibly gives recession proportional to separation, but *insertion* is not *stretching*: cells grow to a fixed maximum size and stop (Sec. 2.1), so the inter-cell spacing is constant by construction and cannot itself stretch a wavelength. Whether inserting cells within a wave's support reproduces $1+z = a_0/a_e$ exactly, rather than approximately, is unverified. And the residual creation excess is here identified with an effective cosmological constant without an argument that the identification is stable under evolution; the emergent-space literature, in which cosmic expansion is likewise the creation of volume [22], derives a Friedmann equation from an equipartition imbalance and is the natural comparison for any successor.

Primordial perturbations: a fired mechanism. The mechanism proposed for primordial density fluctuations was that they are the cell-density statistics of the foam frozen in at the moment of saturation. Disordered jammed packings are *hyperuniform*: the Torquato–Stillinger conjecture, that all saturated, strictly jammed sphere packings have vanishing long-wavelength density fluctuations, has no known counterexample, and maximally random jammed packings show the structure factor vanishing *linearly*, $S(k) \propto k$ as $k \to 0$ [21]. Since $P(k) \propto k$ is the Harrison–Zel'dovich scale-invariant spectrum, a near-linear $S(k)$ at saturation would be a structural echo of the observed primordial form.

The mechanism is falsified on amplitude, and the arithmetic is short enough to state in full. For a hyperuniform packing the number variance in a region of radius R scales as R^2 rather than R^3, so the relative density fluctuation is

$$\delta(R) \;\sim\; (R/\ell_P)^{-2}. \tag{31}$$

A comoving scale of 1 Mpc, evaluated at the Planck epoch ($1+z \simeq 5.2 \times 10^{31}$), has physical radius 5.9×10^{-10} m, i.e. $R/\ell_P \simeq 3.7 \times 10^{25}$. Hence $\delta \sim 7 \times 10^{-52}$, against the required 10^{-5}: a shortfall of forty-six orders of magnitude. The result is not rescued by abandoning hyperuniformity, since ordinary Poisson statistics give $\delta \sim N^{-1/2} \simeq 4 \times 10^{-39}$, still thirty-three orders short.

The shortfall has a clean interpretation. To obtain $\delta \sim 10^{-5}$ the comoving megaparsec scale would have to have been $\simeq 316\,\ell_P$ at saturation rather than $3.7 \times 10^{25}\,\ell_P$, which requires a further factor $\sim 10^{23}$ of expansion — about fifty-three e-folds. *The amplitude gap is the inflation gap.* Inflation supplies the horizon solution and the perturbation amplitude from one mechanism; mode 1 supplies the horizon solution by a route that does not stretch anything, and therefore does not earn the amplitude as a by-product.

This falsifies the packing-statistics origin of primordial perturbations as formulated. It does not touch the two-mode ontology, the horizon-problem argument, or anything in Secs. 2–4. It does fire the primordial-perturbations row of Table 1, and Sec. 9 grades it accordingly. Two further gaps stood behind the amplitude and are recorded for completeness, since any successor inherits them: *scale*, in that $S(k)$ of Planck-scale cell centers and $P(k)$ at comoving megaparsec scales are separated by some sixty decades with the transfer asserted rather than sketched; and *tilt*, in that the measured $n_s = 0.965$ lies many standard deviations below exact scale invariance, so a packing spectrum with a fixed exponent and no tilt mechanism would be falsified by the red tilt even had the amplitude worked.

$S(k)$ of the cell centers at saturation remains worth computing, now as a structural property of the medium rather than as a cosmological entry point: it characterizes the packing the rest of the model is built on, and it is measurable on the same rigs as Secs. 2.3 and 7.2.

Remark 16 (What this sector is, and one tension it inherits)**.** *No Friedmann-like evolution law, no big-bang nucleosynthesis check, no acoustic peak structure, and no growth of structure has been attempted. Precision cosmology is unforgiving, and this section should be read as an ontology with two recorded negative results, not as a cosmological model.*

One tension deserves to be recorded rather than discovered later, because it couples this section to Sec. 2.3. The horizon-problem argument above wants the saturated packing to be maximally uniform*, and hyperuniformity is exactly the property that suppresses long-wavelength density fluctuations. But a Poisson sprinkling is the discretization that admits no preferred frame, precisely because its number variance scales as the volume and it possesses arbitrarily close pairs; a packing with a characteristic spacing and* suppressed *long-wavelength variance is further from that case, not nearer [23]. The foam is therefore being asked to be more ordered than Poisson for this section's purposes and less structured than a lattice for Sec. 2.3's. Whether both are simultaneously available is open, and the convergence measurements of Sec. 2.3 probe one side of it.*

7 Speculative extensions (not used by the chronometry or gravity sectors)

Everything in this section is more hypothetical than the rest of the model, and everything in it is separable: the chronometry, gravity, and expansion sectors of Secs. 2–6 stand or fall independently of anything below. What follows are three extensions (a pair-creation reading of popping, a gross-versus-net vacuum ledger, and a mechanism sketch for quantum events), each stated with its boundary conditions and falsifiable targets.

7.1 Pair creation, antimatter, and the mirror universe

The core mechanics of Sec. 2.1 needs a pop to do nothing but return volume. The extension explored here is that **each pop releases a matter–antimatter pair**, with energy increasing with the size of the cell at the moment of popping. As a working form we adopt the linear law

$$E \;=\; E_P\,\frac{\ell_{\text{pop}}}{\ell_P}, \tag{32}$$

so that a full-size pop carries one Planck energy and an early pop a proportionally small one. Equation (32) is an *ansatz*, a normalization chosen for economy rather than derivation; the ledger below records the observables that constrain it.

Pair fates differ by mode. The pairs released by popping (Sec. 2.1) meet different worlds. A pair born in mode 2 is born under frames: the partners remain adjacent, annihilate within a few ticks, and return their energy; popping in the frame era is the engine of *vacuum fluctuations*, virtual pairs as short loans from the void, repaid at annihilation. A pair born in mode 1 is born into the clockless lateral growth, and its fate follows from the chronometry postulate rather than from any process: all matter dynamics is frame passage (Postulate 2), no frames pass through anything in mode 1, so a mode-1 pair is *frozen inventory*: it cannot interact, and in particular it cannot annihilate, because annihilation is dynamics and mode 1 has none. The partners are separated positionally, generation by generation, by the nucleation of intervening cells (an ordering, not a motion, Sec. 2.2); popping in the clockless era mints *real* particles. The matter content of the universe is the frozen inventory of mode 1, thawed at saturation once frames, and with them dynamics, arrive.

Two directions, two universes. Extrusion into the fourth dimension need not choose a side: the saturated sheet produces frames in *both* four-dimensional directions, and a second stack grows in $-F$, mirror to ours (Fig. 2). The sorting principle is directional preference: of the inherited mode-1 inventory, unconstrained antimatter takes the $-F$ direction of frame development while matter takes $+F$. The result is a mirror universe carrying antimatter equal to our matter, with matter–antimatter symmetry exact globally and broken only by separation. Two experimental boundary conditions hold by construction. Locally, antimatter *bound into our frame development* is swept forward with everything else and gravitates normally, consistent with the observed free fall of antihydrogen [16]; this is automatic, because the gravitational coupling of Postulate 5 reads the *magnitude* of the delivered rotation (energy density) and is blind to its sense. That blindness, however, cuts against the sorting principle and the tension must be owned rather than smoothed over: the reversed rotation sense of antimatter (Sec. 7.3) must be dynamically potent at the sorting epoch (strong enough to segregate the entire cosmic inventory by extrusion direction) and dynamically inert ever after. The model does not yet supply the sense-sensitive interaction that operates only at the mode-1→mode-2 transition; "the directional preference acts only on the unconstrained inventory at the sorting epoch" is at present a description of what is needed, not a mechanism, and it goes on the ledger as such. Globally, the mirror's antimatter occupies the opposite frame direction rather than distant regions of our space, so the gamma-ray annihilation signatures that exclude spatially mixed matter–antimatter domains [13] are absent by construction. Architecturally this is the CPT-symmetric universe/anti-universe pair of Boyle, Finn, and Turok, and the two-armed arrow of time of Barbour's Janus point [14, 15]; the foam contributes a mechanism (bidirectional extrusion) and a sorting principle (directional preference of unconstrained antimatter).

Matter from the timeless phase. Mode 1 answers a question inflation does not: where the matter comes from. The standard account requires a baryogenesis mechanism satisfying the Sakharov conditions [12], in particular CP violation strong enough to leave one part in $\sim 10^9$ unannihilated, which no confirmed mechanism yet supplies. Here the asymmetry is not generated but *sorted*: pairs minted in the timeless mode survive intact, matter taking $+F$ and antimatter $-F$ at saturation (Sec. 2.2), so our universe inherits matter and the mirror inherits antimatter with nothing violated. Quantitative targets follow: the inherited matter density ρ_m is set by the mode-1 popping statistics together with $E(\ell_{\mathrm{pop}})$, and the baryon-to-photon ratio $\eta \simeq 6 \times 10^{-10}$ is then a derived quantity once the early mode-2 annihilation photon budget (the radiation era, in this picture) is computed against the inherited inventory. Neither computation has been attempted; both are well-posed.

The ansatz leaves unanswered: what determines particle species, spin, charge, and momentum at a pop, how the conservation laws emerge, and why the inherited spectrum contains the observed discrete masses. All of this is open; the extension earns its keep only through the ledgers below.

7.2 The zero-point ledger

Energy bookkeeping of popping. The single function $E(\ell_{\mathrm{pop}})$ introduced above is constrained from three independent directions, and the tension among them is itself informative. (i) *Vacuum:*

mode-2 pairs are loans repaid at annihilation; if the books balance exactly, the vacuum does not gravitate at the naive scale, a structural response to the cosmological-constant problem, and the small residual ε of the expansion sector is the net imbalance, not the gross activity. (ii) *Heating:* the destruction halo of Sec. 5.3 is, in this light, a pair-production halo around every mass, running at $\sim 6 \times 10^{101}$ pops $\mathrm{m}^{-3}\,\mathrm{s}^{-1}$ at Earth's surface; Earth's internal heat budget ($\sim 4 \times 10^{-8}$ $\mathrm{W\,m}^{-3}$) then bounds the *net* energy deposited per halo pop below $\sim 7 \times 10^{-110}$ J, ninety-six orders of magnitude below an electron mass. Halo and mode-2 popping must be energy-neutral to extraordinary accuracy: the balanced-loan reading is not optional but forced. (iii) *Matter:* real, unreturned energy enters only through mode-1 pairs, whose statistics must reproduce ρ_m. One function, three ledgers; the mechanism survives only if a single $E(\ell_{\mathrm{pop}})$ serves all three.

Point (i) has epistemic limits: "balanced loans do not gravitate" is at this stage a bookkeeping principle, not a derivation. Promoting it to one requires an effective stress-energy calculation showing why the gross activity sources local vacuum phenomenology (Casimir forces, the Lamb shift) while cancelling gravitationally up to the residual ε. That calculation is open, and the cosmological-constant claim below should be read in that light.

The vertex-count identity and the zero-point sector. The popping rate is not a free parameter: with gapless frames and vertex nucleation (Sec. 2.1), every vertex nucleates a candidate and the survivors number exactly the next frame's cell density, so

$$\text{pops per volume per frame} \;=\; n_{\mathrm{vertex}} - n_{\mathrm{cell}} \tag{33}$$

as an identity. Foam topology makes the right side large and computable: for Poisson–Voronoi statistics (27.07 vertices per cell, each shared by four cells; the exact face count $48\pi^2/35 + 2 \approx 15.535$ is due to Meijering [17]), $n_{\mathrm{vertex}}/n_{\mathrm{cell}} \simeq 6.8$, i.e. $\simeq 5.8$ pops per surviving cell per frame; *most nucleations pop*, and the vacuum is correspondingly furious. The accounting then splits cleanly into gross and net. *Gross (popped ledger):* the standing density of in-flight virtual pairs is $(n_{\mathrm{vertex}}/n_{\mathrm{cell}} - 1)\, k\, n_0 \langle E_{\mathrm{pop}} \rangle$ with k the pair lifetime in ticks; for mean pop fractions $\langle \ell/\ell_P \rangle \sim 0.1$–$0.5$ this is 10^{113}–$10^{114}k$ $\mathrm{J\,m}^{-3}$, the notorious Planck-cutoff zero-point value of quantum field theory ($\sim 10^{112}$–10^{114} $\mathrm{J\,m}^{-3}$), produced here on purpose: real and locally felt (Casimir, Lamb shift), but balanced loans that do not gravitate. *Net (survivor ledger):* survivors are overwhelmingly replacement; dark energy is the residual creation excess ε, and the measured ratio $\rho_\Lambda/\rho_{\mathrm{ZPE}} \simeq 10^{-122}$ equals $(H_0 t_P)^2 = 1.5 \times 10^{-122}$ at order unity. That equality should not be advertised as a success: it is arithmetic available to *any* framework with a Planck cutoff and the measured H_0; it is the standard statement of the cosmological-constant problem, rewritten. What the ledger contributes is only a candidate *reason* for the spread (gross activity locally felt, net imbalance gravitating), and that reason stands or falls with the balanced-loan principle of point (i), which remains undemonstrated. The cosmological-constant problem becomes, conditionally, the gross-versus-net spread of one process. Both sides are measurable in simulation: the foam's $n_{\mathrm{vertex}}/n_{\mathrm{cell}}$, and the sharper target, the pop-size distribution $f(\ell)$, which under the linear law maps to an energy spectrum that must coarse-grain to the ω^3 form, shown by Marshall and by Boyer to be the *unique* Lorentz-invariant zero-point spectrum [18]; any other coarse-grained spectrum would render the substrate detectable in the vacuum sector, extending the invisibility requirement of Theorem 1 beyond chronometry. Boyer's analysis carries a further condition, and it must be stated in the direction it actually points: Lorentz invariance requires the spectrum's *cutoff* to be the same for all inertial observers. A substrate at rest in the CMB frame does *not* automatically supply this, since a cutoff defined in the substrate frame is the prototypical observer-*dependent* cutoff, Doppler-shifted for any moving observer; cutoff invariance is therefore not a freebie of Planck-cell structure but a second invisibility requirement the vacuum sector must *earn*, the analogue for the zero-point spectrum of what Theorem 1 earned for chronometry. Together with the ω^3 form this makes a severe double constraint, and the foam has no obvious a priori reason to satisfy either; that is what makes the pop-size histogram worth taking. It is important to note that we use Boyer's spectral-uniqueness result; we are not adopting the SED program, whose known failure to reproduce nonlinear and entangled systems we do not inherit, because our quantum sector is non-classical.

7.3 Quantum events: instantiation, spin, and lock

The cycle has four stages.

Instantiation. Energy comes into existence in a specific cell of a specific frame, the *progenitor*, and stays there. The progenitor is a fixed point in the block, comoving with the substrate; it does not recede into a dead past but persists in its frame. Let us be precise about what this amends. The core ontology (Secs. 2.2, 3.1) states that past frames carry no *matter*, and this section keeps that: *matter*, the driven choreography that detectors, rulers, and observers are made of and interact with, resides in the current frame, always. But the core also read past frames as inert structure, and the present mechanism *modifies* that reading rather than refining it: a persisting, spinning, lock-funding progenitor is a past-frame entity that is dynamically alive, in live causal contact with the present through its volume-overlap descendant network. This is a substantive speculative amendment (past frames host anchored energy, though never matter), and it stands or falls with this section (the core sections were worded to leave the door open, Sec. 2.2). A particle is then both at once: block-anchored energy plus the surface-riding pattern it drives, with the anchor reset to the present at every lock.

Spin. The progenitor rotates, at the rate set by its energy. This is the fixed-cell phase law of Sec. 5 (Eq. (20)), here anchored at a single substrate-comoving cell, for which processed and substrate frames coincide, so the two readings of "per frame" agree:

$$\chi_E = \frac{E}{E_P} \text{ radians per substrate frame,} \qquad \frac{\chi_E}{t_P} = \frac{E}{\hbar} = \omega, \tag{34}$$

recovering Eq. (18) at $E = mc^2$ and giving a photon its frequency exactly (a 2.5 eV green photon: $\chi_E = 2.05 \times 10^{-28}$ rad per frame, $\omega = 3.80 \times 10^{15}$ rad s^{-1}). An antiparticle is the same construction with the rotation sense reversed, the mechanical content of the Feynman–Stückelberg picture; the reversed sense is the natural microscopic *tag* for the directional sorting of Sec. 2.2 (opposite rotation preferring the opposite direction of frame development), though the dynamical mechanism by which sense couples to extrusion direction at the transition, while remaining gravitationally inert thereafter, is the open item recorded in Sec. 7.1. Under the linear pop-energy ansatz (32), the rotation angle acquires a second geometric reading: $\chi_E = E/E_P = \ell_{\text{pop}}/\ell_P$: *the angle a particle turns per frame equals the fractional size of the cell whose pop minted it.* An electron is a cell that popped at 4.185×10^{-23} of Planck size; that same number is its rotation per frame. Mass, pop size, and rotation rate are one quantity. The reading carries a recorded cost: it assigns the electron a pop size of $4.185 \times 10^{-23}\,\ell_P \approx 7 \times 10^{-58}$ m, twenty-three orders below the cells the model treats as primitive. Either ℓ_{pop} is an internal parameter with no resolved geometric meaning, or the linear ansatz (32) needs a different dimensionless carrier; a derivation must settle which.

Propagation. Nothing travels except motion. The progenitor is coupled to its volume-covering descendants, they to theirs, and a distributed drive is transferred through the weighted overlap network. Sec. 2.3 gives this network a one-cell-per-frame locality bound whose macroscopic limiting speed is intended to converge to c. Choreography fills space; the energy never leaves the instantiation cell. The geometrical overlap rule alone does not license copying a complete quantum state into every descendant. The propagated object must be a distributed amplitude or drive updated by a norm-preserving rule; deriving that unitary or isometric map is an explicit target of this speculative sector. Subject to that boundary, three standard wave properties are suggested by the geometry: a descendant at distance r receives the drive with a lag of r/c, so the phase it carries is the retarded $e^{i(kr-\omega t)}$; every driven descendant contributes to its overlap descendants, which is Huygens' construction discretized at the Planck scale; and the cone surface at radius r contains $\sim 4\pi(r/\ell_P)^2$ cells (4.8×10^{70} at one metre), so each cell's share of the driven energy, an intensity-like quantity, dilutes as $1/r^2$: inverse-square flux without further input. An amplitude would fall as $1/r$; which quantity the update rule conserves awaits the norm-preserving map.

Propagation in a flowing foam. This passage keeps the historical flow carrier; its conclusions about cone advection, horizons, and gravitationally modified propagation are conditional on the successor gravity mechanism (Sec. 5 status note). One subtlety looks at first like a flaw. The descendant cone is perfectly spherical *relative to the cells*, and the cells move. Each generation, the next-frame cells overlap the parent's final volume after the local remeshing step (Sec. 5); so per tick the cone widens by one layer *and its center is advected by* $\mathbf{v}(x)$. In static coordinates the cone is off-center and tipping, the Painlevé–Gullstrand light cones. The quantum wave bends around masses, is Shapiro-delayed, and is redshifted, by exactly the amounts of Sec. 5, because the wave's geometrical carrier and the causal structure are the same object: the volume-overlap network. (In standard physics, "quantum fields propagate on curved spacetime" is a postulate appended to general relativity; here it is forced.) Sphericity in *static* coordinates holds only for an in-place-healing foam, the same fork as Sec. 5; the quantum and gravitational sectors stand or fall together on the single commitment to migratory healing. One further consequence: a horizon is an overlap-network trap. Inside r_s the inflow exceeds one cell per tick, so even the outermost descendants of an interior progenitor move inward (the outgoing cone edge freezes exactly at r_s and plunges inside it); no overlap-descendant path crosses the horizon outward; hence no offer reaches an exterior absorber and no lock can complete across it. A black hole is transactionally silent. That conclusion must immediately be confronted with the literature this paper leans on elsewhere: the central result of the analog-gravity program [7] is that flow horizons in discrete or molecular media generically *radiate* Hawking-fashion, arguably *because of* their microstructure. The foam therefore faces a fork it cannot defer indefinitely. Either the overlap-network microdynamics produces the mode conversion at the horizon that Hawking emission requires, in which case "transactionally silent" is wrong as stated and the mechanism must say how the emission is carried; or it does not, in which case the absence of Hawking radiation is a distinctive (if presently untestable) prediction that separates this model from semiclassical gravity and from its own acoustic-metric relatives. The question is well-posed on the simulated foam (does a translating super-c flow region convert overlap-network drive modes at its boundary?) and is added to the open ledger below.

Lock. When a cell carries drives from two different sources that are phase-compatible and energy-compatible, it *locks*: the energies of both progenitors are transmitted and combine into new instantiation(s), and the cycle repeats. The lock is the quantum event, discrete and all-or-nothing. **Collapse is the silence after the lock**: the energy having transferred, nothing drives the progenitor's rotation any longer, and the entire driven overlap network falls quiet;

the silence is provisional on the open conserved-carrier question (Sec. 5). Collapse is a physical process with a definite locus, the hub, not a rule appended to the formalism. Wave–particle duality acquires a mechanical reading: the wave is the spreading rotation; the particle is the lock.

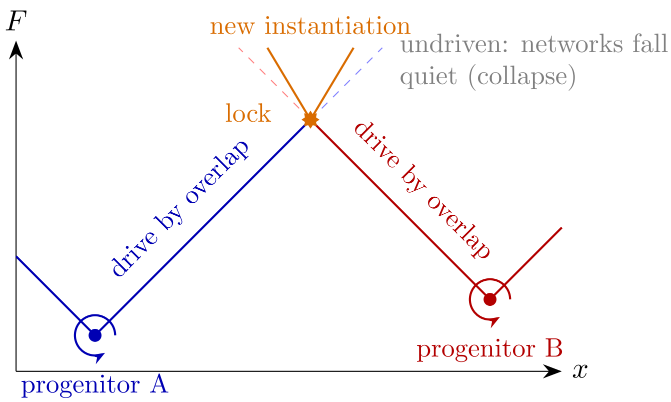

Figure 11: Instantiation, spin, lock. Each progenitor's energy stays in its instantiation cell, spinning at E/E_P radians per frame; the distributed drive propagates through the volume-overlap descendant cones (the candidate light cones of Sec. 2.3). Where the two drives meet phase- and energy-compatible, a lock (star) transfers the energies into new instantiation(s). With nothing driving them, the old driven networks fall quiet (dashed): a physical collapse with a definite locus.

7.4 Lineage, and the two named targets

This mechanism has a lineage: it is structurally a Planck-scale realization of Wheeler–Feynman absorber theory and, more closely, of Cramer's transactional interpretation [11]; emission as offer, absorption as confirmation, the quantum event as a completed handshake rather than a bullet in flight. The lock *is* the transaction. The lineage also locates the hard problems, which we state as deliverables rather than hide.

Target 1: the Born rule. When several distant absorbers are all compatible, what selects the one that locks, and why with probability $|\psi|^2$? The mechanism has one structural asset here: the lock is a *two-wave* condition, the meeting of the emitter's drive and a counter-wave from the candidate absorber, so the lock rate is *bilinear* in the two amplitudes, and bilinearity in offer $\times$ confirmation is the algebraic shape of the Born rule. If the foam dynamics makes lock probability proportional to that product, $|\psi|^2$ ceases to be a postulate. Interference comes along with the same machinery: a cell reachable from one progenitor by multiple overlap paths (two slits) receives drives with different lags, the drives add as phases *before* any lock, and a quadratic lock rule then produces fringes. This is implementable as an algorithm on the simulated foam: amplitudes transferred through the weighted overlap network, summed per cell, and locked quadratically. One caution for that implementation, inherited from the gross bookkeeping of Sec. 7.2: most nucleated candidates pop ($\simeq 5.8$ per surviving cell per frame, and the live rig measured a candidate pop fraction of 0.83). Because descent is assigned only after the next frame closes, this gross attrition does not extinguish the overlap graph. The algorithm must still specify a normalization-preserving update and verify that phase coherence survives remeshing rather than assume it.

Target 2: Bell correlations with no-signaling. The architecture here is meshed anchors. An entangled pair is two progenitor cells instantiated in direct contact, and contact is a constraint: two touching cells cannot spin independently. The foam's two adjacency types then furnish the two extremal state families. *Lateral* mesh (two anchors minted side by side in the same frame) forces counter-rotation, the anticorrelated (singlet-like) family; *vertical* mesh (two anchors in successive frames linked by positive-volume overlap) forces co-rotation, the aligned family. One corollary comes free: since every pop mints an adjacent opposite-sense pair (Sec. 7.1), pair production creates laterally meshed, maximally entangled pairs automatically, as a consequence of adjacency at birth rather than an added postulate. (Three mutually touching anchors would be a native GHZ state.) The picture requires one extension the model needs anyway, recorded on the spin ledger below: the *orientation of the rotation plane* becomes a spatial degree of freedom (the spin axis), while the sense within the plane remains the matter/antimatter tag; the mesh constrains the partners' planes to be parallel with senses opposed (lateral) or aligned (vertical).

Individually, each anchor's orientation is not merely unknown but indefinite: the plane tumbles in a wild dance, and only the *joint* figure is constrained. The dance earns its keep at the marginals: an isotropically tumbling axis gives 50:50 outcomes along *any* analyzer direction, mechanically. What the dance cannot do is carry the correlations, and the exclusion is quantitative. If outcomes were read off a definite instantaneous shared axis, the model would be a stochastic local-hidden-variable theory: Monte Carlo of that reading gives the linear correlation $E(\theta) = -1 + 2\theta/\pi$ (-0.500 at $45°$ against the measured quantum -0.707) and is capped at the CHSH bound of 2 against the observed $2\sqrt{2}$. Worse, the dance decorrelates on the frame timescale while the two locks complete at different substrate times, so a sampling picture yields no correlation at all. Entanglement cannot be a matched dance that measurements *sample*.

The mechanism is instead a *snap*. The first lock in substrate order, completing on one partner along analyzer axis $\mathbf{a}$ with outcome A, breaks the joint dance: the meshed partner's plane takes the definite matched orientation ($-A\,\mathbf{a}$ lateral, $+A\,\mathbf{a}$ vertical), an orientation *created by* the lock, referring to that lock's axis, and therefore not a Bell-forbidden pre-existing answer sheet but the mechanical face of quantum steering. The channel that transmits it is the mesh itself: one cell-contact wide, resident in the creation frame of the block, ageless, and indifferent to the interval between the two locks. This is the active nonlocal coupling a Bell-violating substrate account requires, and it is vertical (block bookkeeping), with nothing propagating spacelike in any current frame. The substrate's absolute simultaneity makes "first lock" well defined even where observers disagree about the order.

The snap decomposes the Bell problem into two stages, and the decomposition has been checked numerically end to end. Stage one, the first lock: 50:50 by the dance's isotropy. Stage two, the second lock: a *single-particle* problem, a definitely-oriented plane meeting an analyzer at relative angle θ, which must obey the Malus/Born rule $\cos^2(\theta/2)$. Assuming only that rule, simulation of the full mechanism (4×10^6 trials per angle) reproduces $E(\theta) = -\cos\theta$ for the lateral family and $+\cos\theta$ for the vertical family to four decimals at every angle tested; reaches CHSH $= 2.828 = 2\sqrt{2}$ at the optimal angles, the Tsirelson bound exactly, neither the classical ceiling nor a super-quantum overshoot, because the structure is self-throttling; returns one-sided marginals of 0.5000 at every analyzer setting, so *no-signaling is structural* rather than imposed (the two snap orientations are equally likely and the Malus rule averages them to $\frac{1}{2}$ regardless of the remote angle); and is order-independent (-0.7071 versus -0.7070 at $45°$ for the two lock orders), so the mechanism's substrate-order asymmetry is statistically invisible, the quantum-sector analogue of what Theorem 1 establishes for chronometry, here verified at the level of outcome statistics for this mechanism. To be exact about claim status: this is a consistency demonstration that the meshed architecture plus the single-particle Malus rule *entails* the quantum correlations; it is not a derivation of Malus from foam dynamics. The entire Bell target therefore collapses into Target 1: derive $\cos^2(\theta/2)$ for one oriented particle against one analyzer from the quadratic lock rule, and Tsirelson-bounded Bell correlations with structural no-signaling follow as corollaries of the mesh.

7.5 Open ledger

Four loose ends remain. *Hawking radiation:* the fork stated above (lineage-trap silence versus the analog-gravity expectation of horizon emission from discrete media) must be resolved by the model's own microdynamics, and the simulated-foam form of the question (mode conversion at a translating super-c flow boundary) is well-posed. *Energy bookkeeping under expansion:* a rotation propagating through frames that gain cells arrives redshifted; if the lock transfers energy at the received frequency, the deficit relative to the instantiated energy needs an account (retained by the progenitor? returned to the void?). General relativity finesses this with frame-dependence; an ontology this concrete must answer. *Spin proper:* the rotation as formalized is a U(1) phase; actual spin-$\frac{1}{2}$, with its 4π periodicity, requires the progenitor's rotation to carry an axis and a richer (SU(2)-like) structure, an extension not yet built. The meshed-anchor account of Target 2 both requires this extension (the rotation-plane orientation is the variable the snap fixes) and gives it work to do. *Competing absorbers:* with collapse physical, the statistics of competing compatible absorbers are in principle calculable within the model and must come out Born; this is where the mechanism is most testable against quantum mechanics, and most at risk.

8 Experimental boundary conditions

Postulates 1–2 exactly fix the smooth ideal-point-clock sector. That sector differs from special relativity only through departures from the postulates or through a specified microscopic accumulator. Other matter and signal equations may contain substrate couplings independently. The principal departure and coupling channels, with their present constraints, are:

(i) Velocity dependence of clock rate. Any first-order-in- v/c term is excluded at the $\sim 10^{-8}$ level or better (optical clocks at 10 $\mathrm{m\,s^{-1}}$; storage-ring muons at $\gamma = 29.3$; Ives–Stilwell-type Doppler tests). The projection law (7) is quadratic at low velocity and survives all of them; the subtraction rule (Remark 1) does not.

(ii) Planck-scale discreteness. Corrections to Eq. (9) of relative order E/E_P generically produce energy-dependent photon dispersion. Time-of-flight limits from the TeV photons of GRB 221009A (LHAASO) now constrain the linear coefficient to $E_{\mathrm{QG},1} \gtrsim 6$–$10\,E_P$, while the best quadratic bound is $E_{\mathrm{QG},2} \gtrsim 6 \times 10^{-8} E_P$ [19]: linear corrections are excluded to beyond the Planck scale; quadratic corrections remain open by nearly eight orders of magnitude and are the natural hiding place for residual substrate signatures.

(iii) The quantum/nonlocal sector. Theorem 1 removes u^μ from the ideal-point-clock proper-time functional but not from quantum foundations. Bell-inequality violations require more than correlations seeded at a shared origin, which alone is a local-hidden-variable scenario, so any substrate account of entanglement needs an *active nonlocal coupling* through the four-dimensional medium, and every known dynamical mechanism of that kind (Bohmian guidance, objective collapse) requires a preferred foliation to be well defined. The frame structure of this model supplies exactly that foliation, and the lock mechanism of Sec. 7 supplies a candidate coupling: the block-resident mesh between co-instantiated anchors, one cell-contact wide, through which the first lock snaps its partner's orientation. Here the substrate frame is not an embarrassment to be hidden but a necessity, and this, not kinematics, is where the model is most distinguishable in principle.

(iv) Sources in spatial superposition. What is the gravitational field of an energy distribution in quantum superposition? Standard physics offers three live answers (a quantized field entangled with the source's which-path state, a semiclassical field sourced by the expectation value $\langle T_{\mu\nu}\rangle$, and gravitationally induced collapse), and no experiment has yet discriminated among them. This model is not neutral: the field follows the actual cell-level events, and the events unfold on the privileged foliation. Under the historical flow implementation the field variable was the cell flow itself; that carrier is falsified (Sec. 5.3), and while a successor mechanism is expected to retain event-defined sourcing, its field variable is not yet fixed. The gravitationally-induced-entanglement proposals now being pursued (Bose et al.; Marletto–Vedral), which would distinguish a quantized field from the alternatives using massive particles in spatial superposition, are therefore in-principle discriminators between this model and quantized-field gravity. The substrate frame, absent from the ideal-point-clock proper-time functional of Theorem 1 and required by the nonlocal sector of paragraph (iii), here acquires its third role: it is what makes "the field of a superposed source" a well-posed question rather than an interpretive one. The model's specific prediction awaits the lock mechanism of Sec. 7 reaching quantitative form, and the claim is bounded accordingly: a prediction channel is identified, not yet a prediction.

9 Claim status

For repository release, the claims stand at different levels:

Claim	**Status**	**Boundary**
Ideal-point-clock Minkowski chronometry	Conditional theorem from postulates	For a smooth additive register, a future-directed timelike path, uniform flow, and flow-rest coordinates, the postulates give standard Minkowski proper time. The square-root law and microscopic accumulator remain underived; full matter-and-signal Lorentz equivalence is not established.

Claim	Status	Boundary
Length contraction	Postulate selected by interferometry	Configuration tilt (Postulate 3) is forced by Michelson–Morley given a real substrate, with Kennedy–Thorndike and Ives–Stilwell closing the dilation–contraction pair. The cell-level (Lorentz–FitzGerald) derivation is open and inherits the wave-sector convergence claims. Operational reciprocity is derived conditionally in Proposition 1 (Sec. 3.7) from Postulates 1–3 plus isotropic signal propagation at c in the substrate frame; the signal law and the cell-level clock and rod dynamics remain underived.
Free motion as stationary register	Postulate; equivalence is a theorem	The extremal law $\delta \int \mathrm{d}\mathcal{N}_{\mathrm{proc}} = 0$ is an independent dynamical input (Postulate 4); given it, equivalence with the geodesic principle follows from Theorem 1. It is not derived from the chronometry postulates.
Phase per frame	Exact Planck-unit representation	Eq. (18) rewrites the standard Compton phase in Planck units, exhibiting the action-phase and energy–frequency roles of $\hbar$; it does not explain the value of the action quantum, and the commutation scale is underived. The open standard is a conserved, quantized cellular rotor action with smallest excitation J_0 identified experimentally with $\hbar$ (Sec. 4.2).
Gravity as Painlevé–Gullstrand flow	Conditional exact correspondence	Given $v(r) = \sqrt{2GM/r}$, the metric reproduces Schwarzschild. The cell-level derivation of that profile from foam mechanics remains open; the certified-medium family is excluded as its source (Sec. 5.3).
Newtonian exponent (flow route)	Negative result in the certified medium	The round-8 campaign found no steady inflow around a sustained sink: the drain refills by local nucleation and the occupancy deficit stays confined within one shell of the drain (Sec. 5.3). The flow route is falsified for this constitutive family; the static-substrate alternative or a new medium class carries the weak-field burden.
Static substrate (retarded nucleation)	Negative result in the certified medium	Retardation moves both dials with the right signs (turnover $\times 0.489$, occupancy $\times 1.354$ at a 50% veto) but at the ratio $\eta_0 = 0.605 \pm 0.058$ where full deflection requires 3: predicted $1.05''$ against the observed $1.75''$ (Sec. 5.3). The static route now requires a spatial carrier that is neither density nor pressure.

Claim	Status	Boundary
Null and moving sources	Stated target; not derived	Postulate 5 fixes the substrate-frame energy-density coupling, with the momentum-tagged sweep of (19) as raw material; the Tolman–Ehrenfest–Podolsky asymmetry and frame dragging must emerge from halo advection (Sec. 5.5). No derivation or simulation yet exists, and the flow route's falsification removed the model's only carrier of $g_{t\varphi}$; the successor requirement is an axial substrate field (Sec. 5.5).
Cosmology (two-mode ontology)	Ontology; no dynamics	The two-mode picture supplies a mechanism for the onset of time and addresses the horizon problem structurally. It supplies no expansion history: a constant creation excess gives de Sitter for all time, and matter consumption carries the wrong sign for the matter era (Sec. 6). A Friedmann-like law is roadmap item 2.
Primordial perturbations	Negative result	The packing-statistics origin is falsified on amplitude: hyperuniform statistics give $\delta \sim 7 \times 10^{-52}$ at comoving megaparsec scales against the required 10^{-5} (Sec. 6). The scale and tilt gaps stand behind it and are inherited by any successor. $S(k)$ at saturation remains worth measuring as a structural property of the medium.
Pair creation, mirror universe, vacuum ledger, lock mechanism	Speculative extensions	These sections define ledgers and tests. They remain separate from the core chronometry and gravity claims.
Experimental boundary conditions	Current literature constraints	The cited bounds should be refreshed before formal submission.

10 Discussion and roadmap

The model now has one conditional theorem it did not have before (ideal-point-clock Minkowski chronometry, Sec. 3.3), one exact correspondence (river chronometry $\leftrightarrow$ Schwarzschild, Sec. 5), one quantitative bridge to quantum mechanics (phase per frame, Sec. 4.2), and one open problem carrying the main load:

1. **Both named routes are answered for the certified family.** The flow route died first: the medium heals in place and drives no steady inflow around a sustained sink. The retardation campaign then measured the static route's first candidate microphysics. It found a genuine transducer, tick and cell count moving together with the right signs, at the intrinsic ratio $\eta_0 = 0.605 \pm 0.058$ where full deflection requires 3 (Sec. 5.3). The open task has changed shape again: a search under four recorded constraints. A successor mechanism must carry its spatial half on something other than density or pressure (both screen within two spacings), deliver three units of space response per unit of tick response in the linear limit, survive the crowding regulator that erased both predecessors, and supply the axial field the Kerr sector demands (Sec. 5.5). Any candidate opens a fresh pre-registration

ledger; both negative results stand on the record in every case.

2. **Covariant flow dynamics.** Promote the cell flow to a field with its own action whose stationary configurations around sinks reproduce (22), whose homogeneous mode carries a constant creation excess (effective Λ) with matter back-reaction, and whose linearization about a moving source reproduces the gravitomagnetic sector, passing the null-limit drag asymmetry of Sec. 5.5: one constitutive law serving both Secs. 5 and 6, with the momentum-tagged deposit of (19) as its source structure. Sec. 6 sharpens the constraint on the homogeneous mode: it must reproduce an expansion history that was fast and decelerating, which the naive reading of matter back-reaction inverts.

3. **Measure the saturation spectrum.** Compute the structure factor $S(k)$ of cell centers in the simulated foam at pressure saturation and examine its small-k behavior. This is now a structural measurement of the medium, not a cosmological one: the packing-statistics origin of primordial perturbations is falsified on amplitude (Sec. 6). Two uses remain. It characterizes the packing the rest of the model is built on, and it bears on the tension of Remark 16, since suppression of long-wavelength variance is what separates this medium from the Poisson case that admits no preferred frame [23]; verify the packing-literature claims in parallel.

4. **Measure the vertex ratio, overlap closure, and the pop spectrum.** The identity (33) makes the gross popping rate a measured topological property: record $n_{\text{vertex}}/n_{\text{cell}}$ of the simulated foam (Poisson–Voronoi benchmark: 6.8). Independently verify the descent closure $\sum_j D_{ij}^{(n)} = 1$, the distribution of overlap weights, and the macroscopic roundness and speed of overlap-descendant cones. Then histogram the pop-size distribution $f(\ell)$: under the linear energy law its coarse-grained spectrum must approach ω^3 (the unique Lorentz-invariant zero-point spectrum [18]) for the substrate to remain invisible in the vacuum sector, a sharp, cheap test that runs on the same data as items 1 and 3.

5. **Implement the lock algorithm.** Realize Sec. 7 on the simulated foam: per-frame rotation (34) transferred through weighted overlap networks, summed per cell, and locked bilinearly with an explicitly norm-preserving update. Targets in order: the free propagator; two-slit fringes; Born statistics with competing absorbers; CHSH correlations with verified no-signaling.

6. **Keep the experimental ledger current.** The bounds cited here (GRB dispersion limits, PPN parameters, antihydrogen gravity, packing hyperuniformity) were verified against the literature as of mid-2026 and should be refreshed at submission; the Boyle–Finn–Turok framework additionally makes ancillary predictions (right-handed neutrino dark matter at 4.8×10^8 GeV, Majorana light neutrinos, a massless lightest neutrino, no primordial long-wavelength gravitational waves) from which the present mechanism should be explicitly distinguished.

Two pre-registered campaigns have now removed the flow route and the retarded-nucleation static route for one constitutive family, and neither touched the chronometry theorem, the quantum bridge, or the two-mode expansion picture. The foam responds to mass on both dials, with the right signs; the campaigns priced that response and found it a fifth of what deflection demands. The question left standing is whether any local rule can respond at triple strength in space against tick, through a carrier its own regulators do not erase. If such a rule exists, one mechanism, cells created, destroyed, flowing, and spinning, may still underlie five things usually treated separately: the relativity of time, the universality of free fall, the expansion of the universe, the phase of quantum mechanics, and, most speculatively, the quantum event itself.

A Notation

Symbols used across more than one section, with the section of first definition. Planck units are $\ell_P = \sqrt{\hbar G/c^3}$, $t_P = \ell_P/c$, $m_P = \sqrt{\hbar c/G}$, $E_P = m_P c^2$.

Symbol	Meaning	Dimensions	First use
t	substrate time (global frame count $\times\, t_P$)	s	Sec. 2.2
F	frame-layer (block) coordinate along the stack, distance $F\ell_P$; mirror stack at $F<0$	—	Sec. 2.2
τ	ideal-clock proper time (smooth processed measure $\times\, t_P$)	s	Sec. 3
σ	ledger advance, $\mathrm{d}\sigma = c\,\mathrm{d}\tau$	m	Sec. 3
$\mathcal{N}_{\text{proc}}$	smooth effective processed-frame accumulator	—	Sec. 3
L_0, L	rest-configuration extent; current-frame footprint	m	Sec. 3.6
θ	ledger tilt angle, $\cos\theta = \sqrt{1 - w^2/c^2}$	—	Secs. 3, 3.
$D_{ij}^{(n)}$	parent-volume overlap weight from frame n to $n+1$	—	Sec. 2.3
$\mathbf{w}$	velocity relative to the local cell flow	$\mathrm{m\,s^{-1}}$	Sec. 3
u^μ	dimensionless unit timelike cell-flow vector	—	Sec. 2.3
$\eta_{\mu\nu}$	Minkowski tensor $(+,-,-,-)$; shorthand, per Thm. 1	—	Sec. 3
n_0	vacuum cell number density, $1/\ell_P^3$	$\mathrm{m^{-3}}$	Sec. 2.1
V, s	vertices per cell; cells sharing a vertex (s=4 in 3D)	—	Sec. 7.2
χ	worldline phase per *processed* frame, m/m_P	rad	Sec. 4.2
χ_E	fixed-cell phase per *substrate* frame, E/E_P	rad	Sec. 5
φ	quantum phase field, $(Et - \mathbf{p}\cdot\mathbf{x})/\hbar$	rad	Sec. 5
S	action, $-\hbar\,(m/m_P)\,\mathcal{N}_{\text{proc}}$	J s	Sec. 4.2
$v(r)$	radial inflow speed of the cell flow	$\mathrm{m\,s^{-1}}$	Sec. 5
δP	pressure deficit of the foam	$\mathrm{J\,m^{-3}}$	Sec. 5
ρ	foam inertial density	$\mathrm{kg\,m^{-3}}$	Sec. 5
A, B	deficit and inflow amplitudes: $\delta P{=}A/r$, $v{=}Br^{-1/2}$	varies	Sec. 5
Q	point-sink volume flux, $\lim_{r\to 0} 4\pi n_0 r^2 v$	$\mathrm{cells\,s^{-1}}$	Sec. 5.3
λ	source efficiency: pops per delivered rotation per frame	—	Lem. 5.4.5
κ	deficit response per unbalanced consumption	—	Lem. 5.4.5
r_s, r_t	horizon radius $2GM/c^2$; turnaround $(2GM/H^2)^{1/3}$	m	Sec. 5
φ_ν, φ_ℓ	static-route tick-rate and cell-size fields	—	Sec. 5
Φ	Newtonian potential	$\mathrm{m^2\,s^{-2}}$	Sec. 5
ε	fractional linear-scale creation excess per frame, $H_0 t_P$	—	Sec. 6
H, H_0	Hubble rate; present value	$\mathrm{s^{-1}}$	Sec. 6
$S(k)$	structure factor of cell centers (distinct from action S)	—	Sec. 6
ℓ, $f(\ell)$	pop size; pop-size distribution	m; $\mathrm{m^{-1}}$	Sec. 7.2
ω	angular frequency, $\chi_E/t_P = E/\hbar$	$\mathrm{s^{-1}}$	Sec. 7

B Numerical values

Planck length	$\ell_P = 1.616255 \times 10^{-35}$ m
Planck time	$t_P = 5.391246 \times 10^{-44}$ s
Planck mass	$m_P = 2.176434 \times 10^{-8}$ kg
Frame rate (rest)	$F_0 = 1/t_P = 1.8549 \times 10^{43}$ s^{-1}
Cell density	$n_0 \simeq \ell_P^{-3} = 2.3685 \times 10^{104}$ m^{-3}
Electron phase per frame	$\chi_e = m_e/m_P = 4.185 \times 10^{-23}$ rad
Electron rest rotation rate	$\chi_e/t_P = 7.763 \times 10^{20}$ rad s^{-1} $= m_e c^2/\hbar$
Frames per electron phase cycle	$2\pi m_P/m_e = 1.501 \times 10^{23}$
Solar-limb deflection (flow / rate-only)	$1.752''$ / $0.876''$
Cassini constraint	$\gamma - 1 = (2.1 \pm 2.3) \times 10^{-5}$
Inflow at solar surface / 1 AU	617.8 / 42.1 km s^{-1}
Earth-surface inflow	11.2 km s^{-1}
Solar horizon radius	$r_s = 2.95$ km
Curvature, closed-shell variant	$\Omega_k \approx -1.1$ (excluded $\sim 580\sigma$)
Measured curvature	$\Omega_k = 0.0007 \pm 0.0019$ (Planck+BAO)
Fractional linear-scale excess per frame	$\varepsilon = H_0 t_P \sim 1.2 \times 10^{-61}$
Green photon (2.5 eV) rotation	$\chi_E = E/E_P = 2.05 \times 10^{-28}$ rad per frame
equivalent angular frequency	$\chi_E/t_P = E/\hbar = 3.80 \times 10^{15}$ rad s^{-1}
Descendant-cone cells at $r = 1$ m	$4\pi(r/\ell_P)^2 = 4.8 \times 10^{70}$
Destruction-halo cutoff $r_t = (2GM/H^2)^{1/3}$	Sun: 121 pc; $10^{12} M_\odot$: 1.2 Mpc; $10^{15} M_\odot$: 12 Mpc

C The one-dimensional flow toy

This appendix documents the toy quoted in Sec. 5, which documents the historical migratory-healing implementation used in the now-falsified flow-route gravity test. Material markers lean inward under migratory healing at the rate continuity demands and do not lean under in-place healing. This appendix is retained as a record of that implementation; it no longer defines the core descent ontology, which is the volume-covering relation of Sec. 2.3.

Model. An incompressible column of cells at unit spacing occupies $x = 1, \ldots, L$ with $L = 400$, with a popping probability per cell per frame $P(x) = p_0 e^{-x/w}$, $p_0 = 0.02$, $w = 30$ (enhanced popping toward $x = 0$). *Migratory healing:* when a cell at x_p pops, every cell at $x > x_p$ shifts inward by one spacing and a new cell is appended at the outer boundary (the source at infinity); cells at $x < x_p$ do not move. *In-place healing:* the popped cell is replaced at x_p; nothing moves. A material marker follows the shifted cells: it moves with the material at its location, i.e. inward by one spacing per pop occurring interior to it.

Prediction. Continuity for the migratory case gives the exact discrete marker velocity $v(r) = \sum_{x=1}^{r-1} P(x)$. The often-quoted continuum approximation $p_0 w(1 - e^{-r/w})$ is systematically high for unit lattice spacing; the table below uses the exact discrete sum. The in-place case gives $v \equiv 0$.

Result (300 falling markers, instantaneous velocity binned by current radius):

r	measured $v(r)$	continuity prediction
30	0.355	0.366
90	0.568	0.560
150	0.594	0.586
210	0.597	0.589
270	0.588	0.589
330	0.590	0.589

Agreement is at the few-percent level; the remaining innermost-bin deficit reflects finite popping discreteness and binning. The in-place mode yields zero. The toy establishes *existence*, the lean is real and equal to the continuity integral, not the exponent: in one dimension flux conservation forces v to saturate, and the $r^{-1/2}$ question is intrinsically three-dimensional. The preliminary 3D local-relaxation test in Sec. 5.3 probes that question; roadmap item 1 records the required robustness checks.

References

[1] J. S. Bell, "How to teach special relativity," Progress in Scientific Culture **1** (1976); reprinted in *Speakable and Unspeakable in Quantum Mechanics* (Cambridge University Press, 1987).

[2] L. C. Epstein, *Relativity Visualized* (Insight Press, San Francisco, 1985); J. M. C. Montanus, "Proper-time formulation of relativistic dynamics," Found. Phys. **31**, 1357 (2001).

[3] H. Reichenbach, *The Philosophy of Space and Time* (Dover, New York, 1958); R. Anderson, I. Vetharaniam, and G. E. Stedman, "Conventionality of synchronisation, gauge dependence and test theories of relativity," Phys. Rep. **295**, 93 (1998).

[4] R. Mansouri and R. U. Sexl, "A test theory of special relativity," Gen. Relativ. Gravit. **8**, 497 (1977); **8**, 515 (1977); **8**, 809 (1977).

[5] P. Painlevé, C. R. Acad. Sci. (Paris) **173**, 677 (1921); A. Gullstrand, Ark. Mat. Astron. Fys. **16**, 1 (1922).

[6] A. J. S. Hamilton and J. P. Lisle, "The river model of black holes," Am. J. Phys. **76**, 519 (2008).

[7] W. G. Unruh, "Experimental black-hole evaporation?" Phys. Rev. Lett. **46**, 1351 (1981).

[8] B. Bertotti, L. Iess, and P. Tortora, "A test of general relativity using radio links with the Cassini spacecraft," Nature **425**, 374 (2003).

[9] C. W. Chou, D. B. Hume, T. Rosenband, and D. J. Wineland, "Optical clocks and relativity," Science **329**, 1630 (2010).

[10] J. Bailey *et al.*, "Measurements of relativistic time dilatation for positive and negative muons in a circular orbit," Nature **268**, 301 (1977).

[11] J. G. Cramer, "The transactional interpretation of quantum mechanics," Rev. Mod. Phys. **58**, 647 (1986); J. A. Wheeler and R. P. Feynman, "Interaction with the absorber as the mechanism of radiation," Rev. Mod. Phys. **17**, 157 (1945).

[12] A. D. Sakharov, "Violation of CP invariance, C asymmetry, and baryon asymmetry of the universe," JETP Lett. **5**, 24 (1967).

[13] A. G. Cohen, A. De Rújula, and S. L. Glashow, "A matter-antimatter universe?" Astrophys. J. **495**, 539 (1998).

[14] L. Boyle, K. Finn, and N. Turok, "CPT-symmetric universe," Phys. Rev. Lett. **121**, 251301 (2018).

[15] J. Barbour, T. Koslowski, and F. Mercati, "Identification of a gravitational arrow of time," Phys. Rev. Lett. **113**, 181101 (2014).

[16] E. K. Anderson *et al.* (ALPHA Collaboration), "Observation of the effect of gravity on the motion of antimatter," Nature **621**, 716 (2023).

[17] J. L. Meijering, "Interface area, edge length, and number of vertices in crystal aggregates with random nucleation," Philips Res. Rep. **8**, 270 (1953).

[18] T. W. Marshall, “Random electrodynamics,” Proc. R. Soc. London A **276**, 475 (1963); T. H. Boyer, “Random electrodynamics: the theory of classical electrodynamics with classical electromagnetic zero-point radiation,” Phys. Rev. D **11**, 790 (1975).

[19] LHAASO Collaboration (Z. Cao *et al.*), “Stringent tests of Lorentz invariance violation from LHAASO observations of GRB 221009A,” arXiv:2402.06009; T. Piran and D. D. Ofengeim, “Lorentz invariance violation limits from GRB 221009A,” Phys. Rev. D **109**, L081501 (2024).

[20] M. Kardar, G. Parisi, and Y.-C. Zhang, “Dynamic scaling of growing interfaces,” Phys. Rev. Lett. **56**, 889 (1986); K. A. Takeuchi, “An appetizer to modern developments on the Kardar–Parisi–Zhang universality class,” Physica A **504**, 77 (2018); S. G. Alves and S. C. Ferreira, “Eden clusters in three dimensions and the Kardar–Parisi–Zhang universality class,” J. Stat. Mech. (2012), arXiv:1209.4385 ($\beta = 0.242$ for radial three-dimensional growth).

[21] S. Torquato and F. H. Stillinger, “Local density fluctuations, hyperuniformity, and order metrics,” Phys. Rev. E **68**, 041113 (2003); A. Donev, F. H. Stillinger, and S. Torquato, “Unexpected density fluctuations in jammed disordered sphere packings,” Phys. Rev. Lett. **95**, 090604 (2005).

[22] T. Padmanabhan, “Emergence and expansion of cosmic space as due to the quest for holographic equipartition,” arXiv:1206.4916 (2012); “Emergence and expansion of cosmic space,” in *Gravitation and Cosmology.*

[23] L. Bombelli, J. Henson, and R. D. Sorkin, “Discreteness without symmetry breaking: a theorem,” Mod. Phys. Lett. A **24**, 2579 (2009), arXiv:gr-qc/0605006; L. Bombelli, J. Lee, D. Meyer, and R. D. Sorkin, “Space-time as a causal set,” Phys. Rev. Lett. **59**, 521 (1987).